UNIVERSITÉ DE SHERBROOKE
Faculté de Génie
Département de Génie Mécanique

ÉTUDE DU RETRAIT DU POLYESTER RENFORCÉ PAR DES TISSUS DE VERRE

INVESTIGATION OF SHRINKAGE BEHAVIOUR OF POLYESTER REINFORCED BY WOVEN GLASS FABRICS

Mémoire de maîtrise en sciences appliquées
Spécialité : Génie Mécanique

Viet Do Thanh

Sherbrooke (Québec), **CANADA**

Février 1999

RÉSUMÉ

Le moulage de composites à renforts tissés sur des formes complexes ayant une double courbure conduit à un réarrangement complexe des différentes couches du stratifié. Ces changements qui se produisent durant la mise en forme modifient les propriétés mécaniques et thermiques du matériau et créent des niveaux de contraintes et déformations résiduelles difficilement prévisibles. Cette étude vise à prédir les facteurs suivant: les coefficients de retrait des composites tissés, le réarrangement des fibres qui s'effectue durant le moulage de formes complexes en composite à fibres tissées, ansi que les contraintes et déformations résiduelles qui en découlent.

Le coefficient de retrait est estimé à partir de la théorie classique des stratifiés et de l'extension non linéaire. La réorientation des fibres et la variation de l'épaisseur des couches constituantes sont prédites en utilisant la méthode du filet à rotules. La variation de l'épaisseur des plis est calculée pour le cas d'un moulage avec matrice simple. Les distorsions de la pièce moulée sont calculées avec un modèle par éléments finis qui tient compte du réarrangement complexe des couches. Un modèle pour la caractérisation du comportement mécanique des composites à renfort tissé, basé sur le modèle mosaïque, est présenté et utilisé pour la modélisation de la structure.

En étudiant le coefficient de retrait, on en déduit que la résine tend à se contracter dans la direction perpendiculaire à la direction des fibres tandis qu'il y a expansion dans la direction des fibres. Pour des laminés fabriqués à partir de tissus non-symétriques tels que le «satin8» et de la résine polyester ayant durci à la température ambiante, il y a une grande déformation

hors du plan du tissu après durcissement. Conséquemment, le coefficient de retrait a été déterminé de deux façons : par la théorie classique des stratifiés et aussi par l'extension non linéaire. Les résultats montrent que la prédiction basée sur la solution non-linéaire est conforme au résultat expérimental.

Les prédictions numériques de la réorientation des fibres, de la variation de l'épaisseur des couches et des distorsions sont comparées avec des pièces moulées sur une forme hémisphérique à base conique. Afin de mettre en évidence les variations de comportement de différents types de tissage, deux composites tissés constitués de fibres de verre et de résine polyester ont été utilisés: une toile et un satin de 8.

Les mesures de l'orientation des fibres et de l'épaisseur des plis ont montré une grande conformité des valeurs calculées avec le modèle numérique du filet à rotules. Une précision légèrement supérieure des résultats a toutefois été observée avec le composite en toile, confirmant le comportement plus uniforme de la toile comparé au satin 8. D'autre part, une plus grande facilité de formage du satin 8 a été observée, ce qui confirme les différences de comportement de plusieurs types de tissés.

L'analyse par éléments finis des distorsions a montré une bonne précision. Le modèle proposé pour la caractérisation mécanique des composites tissés s'est avéré efficace lors de l'analyse.

SUMMARY

Forming of fabric composites into complex parts such as double curvature shells leads to complex redistribution and reorientation of fibres in the composite. This results in heterogeneity in thermal and mechanical properties of the material which in turn creates residual stresses and deformation of the part after moulding. This study deals with the prediction of the shrinkage coefficient of fabric composite, the fibre reorientation and layer thickness variation during forming of fabric composites as well as the resulting residual stress and deformation after moulding.

The shrinkage coefficient is evaluated using the classical laminate theory and the non-linear extension. The fibre reorientation is predicted using the pin-jointed net theory. The layer thickness variation is calculated according to single die moulding. A finite element model using calculated rearrangement of the laminate is generated for the residual distortion prediction of the complex part. A model for the analysis of the mechanical behaviour of fabric composite, based on the mosaïc model, is presented and used in the finite element model.

The investigation of shrinkage coefficient leads to the conclusion that the resin tends to shrink in the direction perpendicular to the fibre direction while it extends in the fibre direction. For laminates fabricated from unsymmetric woven fabric such as 8 harness satin and polyester resin with room-temperature curing, there is a large out-of-plane deformation in the after curing. The determination of the shrinkage coefficients was realised in two ways: by using the classical laminate theory and the non-linear extension. The results showed that the prediction based on the non-linear solution conforms to the experimental results.

The prediction of the rearrangement of the laminate and the distortion were compared to experiments on rounded top cone parts. To study the influence of behaviour of the fabric

structures, two different glass polyester fabric composites were used: plain weave composite and 8 harness satin. Experimental measurements of the fibre orientation and thickness of the moulded parts showed good agreement with the predictions. As expected, uniformity of the rearrangement on the plain weave composite parts and better formability of the 8-harness satin weave composite have been observed.

The finite element computation of the distortions of the moulded parts show good agreement with experimental measurements. The model for the mechanical behaviour of fabric gave relatively good results.

ACKNOWLEDGEMENTS

I would like to express my deep gratitude to my supervisor Prof. Toan Vu Khanh for his trust, guidance and advice throughout the course of this thesis. I am also very grateful to Eng. Tremblay Magella for all the time he spent with me on almost every aspect of this work. Thanks are also due to Eng. Yves Baillargeon for his collaboration to use his program.

I am very grateful to my sister for her love, support and encouragement. Also, my deepest love to my wife Nguyen Thi Kim Dung, who, in understanding what this thesis means to me, has accepted that we can be separated for a while in the hope of a better future.

Finally, I would like to express my sincere thanks to the Mechanical Engineering Department of the University of Sherbrooke for the financial support.

TABLE OF CONTENTS

LIST OF FIGURES

LIST OF TABLES

LIST OF SYMBOLS

fs :	fibre spacing
dps :	data point spacing
l :	length between the adjacent meshes
θ :	angle of ply orientation
s :	corrective factor
t, t_0 :	thickness of a ply
σ_i :	stress component
ε_i :	strain component
ε^0_i :	strain component in mid-plane
Q_{ij} :	stiffness coefficient
$Q_{ij[eq]}$:	equivalent stiffness coefficient
A_{ij}, B_{ij}, D_{ij} :	stiffness modulus of laminate
$A^s_{ij}, B^s_{ij}, D^s_{ij}$:	stiffness modulus of laminate
a_{ij}, b_{ij}, d_{ij} :	compliance of laminate
M_i, N_i :	moment and force resultant
k_i :	curvature
z :	coordinate in thickness sense
u, v, w :	mid-plane and out-of-plane deformation
n_g :	geometrical parameter of woven fabric pattern
T :	temperature
$\gamma_l, \gamma_{nl}, \gamma_{nls}$:	shrinkage coefficient from linear analysis, zero in-plane non-linear analysis, in-plane non-linear analysis
α :	cone angle

W :	potential energy
R :	radius of hemisphere
L :	length of a repetitive unit of fabric
e :	intermediate thickness in sub-plies model
E :	Young`s modulus
G :	shear modulus
x, y, z :	cartesian coordinate

CHAPTER 1

INTRODUCTION

INTRODUCTION

In recent years, applications of reinforced polyester have increased constantly in various fields such as automobile, construction, marine, sanitary equipment, etc. Polyester reinforced by glass fibre, indeed, offers major advantages including low cost tooling, ease of fabrication, wide range of available colours, light weight, high strength, high choke resistance, simple curing cycle, etc. However, several problems related to the quality of parts made of polyester reinforced by glass fibre such as warpage, surface appearance, crack initiation etc. are frequently encountered in practice. This is caused by shrinkage during polymerisation of the resin. Much works [1-9] have been carried to reduce shrinkage of polyester resin. However, these reported works are limited to polyester film or short fibre composites. There are not any investigation on the same phenomenon for the woven fabric composite. To predict the shrinkage of polyester reinforced with woven fabric, the following problems need to be addressed:

- To choose the mathematical model for modelling the mechanical properties of woven composite.
- To determine the shrinkage coefficients.

Deliberate efforts have been made to model the mechanical performance of woven fabric composites. The various mathematical models such as the mosaic model, the fibre undulation model, bridging model and sub-plies model have been developed. These models, incorporated with the classical laminate theory were used to predict the thermal and the mechanical properties of woven fabric composite. However, the mosaic model, the crimp model and the bridging model cannot be applied to the case of non orthogonal fabric structures, encountered in parts with double curvature. The sub-plies model will thus be utilized in this work.

Although the polymerisation of polyester occurred at room temperature, problems such as warpage and large out-of-plane deformation, encountered in composite with high curing

temperature, were also observed in composite made of polyester. Therefore, the shrinkage coefficients can be determined in the manner of the thermal expansion coefficients.

It is known that, during the fabrication process, due to the mismatches of the thermal coefficients or the shrinkage coefficients between two directions: longitudinal and perpendicular to the fibres, laminates experience very complex changes in shape.

If the lay-up configurations are not symmetric about mid-plane of the plate, a bent or warped shape due to bending-stretching and bending-twisting coupling occurs. Experiments [10] showed an appearance of circular cylindrical shape rather than saddle shape for laminate. On the other hand, the out-of-plane deformations of thin laminate are many times higher than of the thickness. As a consequence, the classical laminate theory is in conflict with the experiments and needs to be modified. The reported investigations [11-18] developed a geometrical non-linear solution from the classical laminate theory to conform to the experiment. However, these efforts have been only offered to the unwoven composites. Following the above approaches, the purpose of this work is to address the shrinkage problem in woven composite made of polyester.

Accordingly, in this thesis, we will address the following issues: First, the theoretical background will be given in Chapter II. Then the methods and the models used to address the shrinkage problem will be presented in Chapter III. The description of the sub-plies model for modelling woven fabric composite, the methods for evaluating the shrinkage coefficients consisting of the linear and non-linear theories, the fisherman'net method for meshing woven fabric, and the finite element method application will be issued. Chapter 4 will be reserved for the experimental results and discussions. We will conclude with a discussion of the main issues addressed in this work.

CHAPTER II

THEORETICAL BACKGROUND

2. THEORETICAL BACKGROUND

2.1 Material composite

Composites consist of one or more reinforcement phases embedded in a matrix phase. The reinforcement phase is usually harder and stronger than the matrix phase. Properties of composites are strongly influenced by the properties of their constituent materials, their distribution, and the interaction among them.

2.2 Matrix materials

Fibres, since they can not transmit loads from one to another, they have to be embedded in a matrix material, to form a composite. The matrix serves to bind the fibres together, transfer loads to the fibres, and protect them against environmental attack and damage due to handling.

2.2.1 Polymers

Polymers are the most widely used matrix material for fibre composites. Their main advantages are low cost, easy processibility, good chemical resistance, and low specific gravity. According to their structure and behaviour, polymers can be classified as thermoplastic or thermosets. Thermoplastic polymers soften or melt on heating. Otherwise, thermosetting plastics do not soften but decompose on heating

2.2.2 Common Polymeric Matrix Materials

Polyester and epoxy are the most common polymeric matrix materials used with high-performance reinforcing fibres. Both of them are thermosetting polymers. The typical properties of polyester and epoxy are listed in table 2.1 and 2.2.

TABLE 2.1 TYPICAL PROPERTIES OF POLYESTER RESIN

Density, g/cm^3	1.1 - 1.4
Tensile strength, MPa	34.5 - 103.5
Tensile modulus, GPa	2 - 4.4
Thermal expansion, $10^{-6}/^0C$	55 – 100
Water absorption, % in 24 h	0.15 - 0.6

TABLE 2.2 TYPICAL PROPERTIES OF EPOXY RESIN

Density, g/cm^3	1.2 - 1.3
Tensile strength, MPa	55-130
Tensile modulus, GPa	2.75 - 4.1
Thermal expansion, $10^{-6}/^0C$	45 – 65
Water absorption, % in 24 h	0.08 - 0.15

2.3 Fibre

A great majority of materials are stronger and stiffer in the fibrous form than as a bulk material. A high fibre aspect ratio (length-diameter ratio) permits very effective transfer of load via matrix materials to the fibres, thus taking advantage of their excellent properties. Therefore, fibres are very effective and attractive reinforcement materials. There are a variety of fibres in the market. However, the following kinds are used widely.

- Glass fibre
- Carbon and Graphite fibre
- Aramid fibre
- Boron fibre

Glass fibres are the most common of all reinforcing fibres for polymer matrix composites. The principal advantages of glass fibres are the low cost and high strength. The disadvantages are low modulus and poor abrasion resistance. Two forms of glass fibres can be produced - continuous fibre and discontinuous fibre. In the continuous form, glass fibre can be classified in two types: nonwoven and woven.

2.3.1 Woven fabric

In the woven fabric, fibre yarn is woven into fabric by standard textile operations. Woven fabric is commercially available in various forms such as plain weave, twill weave, crowfoot satin, 5 harness satin and 8 harness satin, figure 2.1.

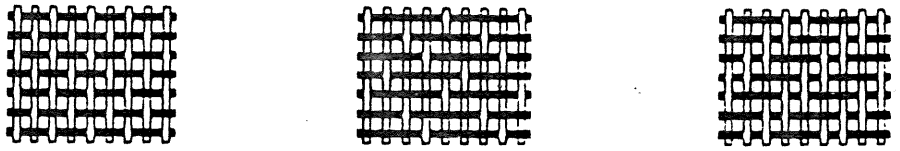

Plain weave crowfoot satin twill weave

5 harness satin 8 harness satin

Figure 2.1 Different types of woven fabric

The various types of fabric structures can be identified by the pattern of their repeating regions. They are characterized by a geometrical parameter n_g, that denotes a warp thread which is interlaced with n_g weft threads, figure 2.2. For example, $n_g = 2$ for plain weave, $n_g = 3$ for twill weave, $n_g = 4$ for crowfoot satin, $n_g = 5$ for 5 harness satin, and $n_g = 8$ for 8 harness satin.

Figure 2.2 The pattern of the repeating region ($n_g = 8$)

2.4 Classification of composite material

Most composite materials developed so far, have been fabricated to improve mechanical properties such as strength, stiffness, toughness, and high-temperature performance. It is natural to study together the composites that have a common strengthening mechanism. The strengthening mechanism strongly depends on the geometry of the reinforcement. Therefore, it is quite convenient to classify composite materials on the basis of the geometry of a representative unit of reinforcement. Figure 2.3 represents a commonly accepted classification scheme for composite materials.

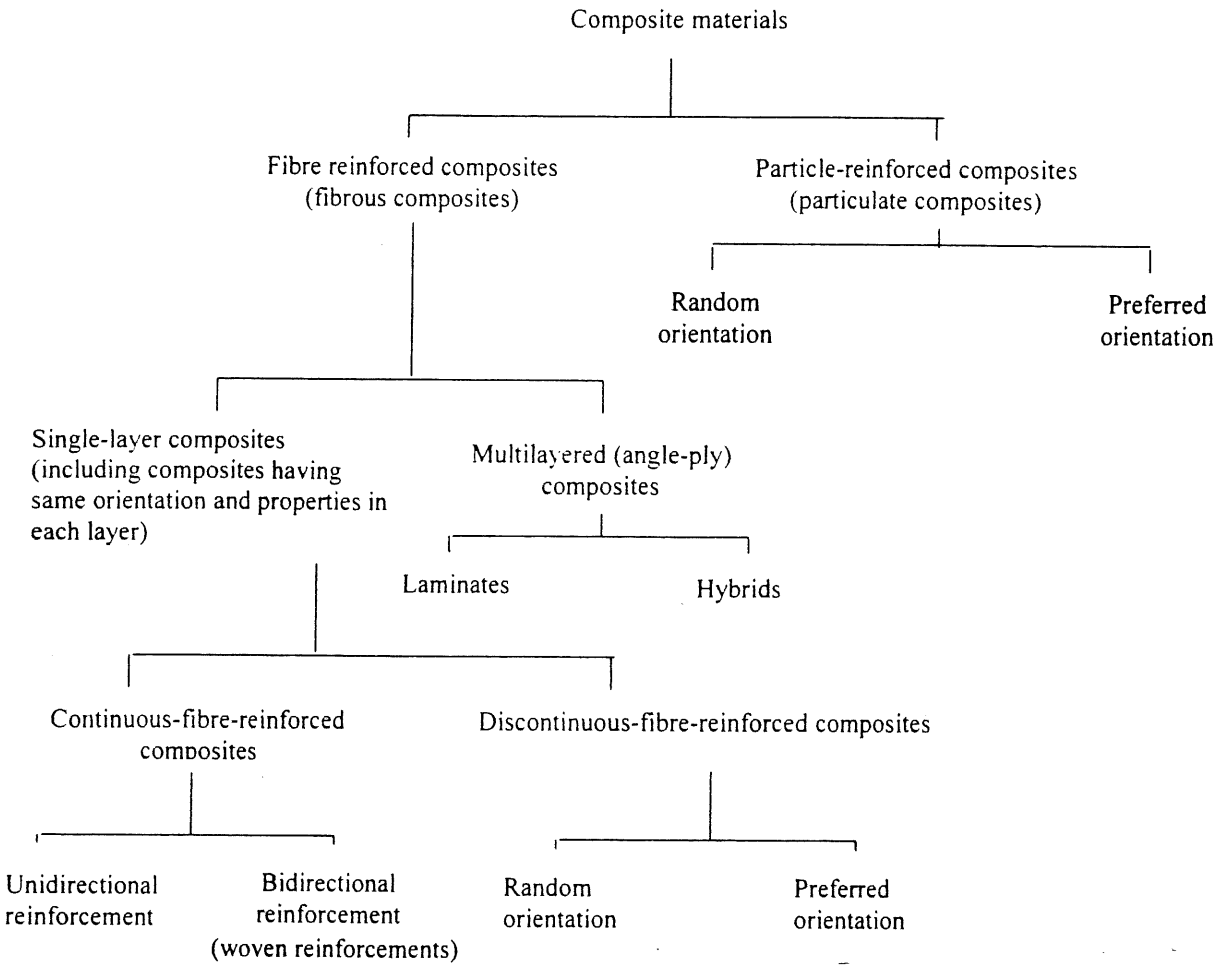

Figure 2.3 Classification of composite materials

2.5 Different types of fibre deformation

During the forming process, the fabric must deform to conform to the die geometry. As a result, the fill threads and the weft threads of fabric are no longer orthogonal. This results in a significant modification of the mechanical properties of woven composite. Thus, the study of the different deformed forms of fabric plays an important role.

2.5.1 Stretching of the fibre

Because the Young's modulus of the glass fibre is about 68.9 GPa and the maximum stretching of fibre is about 4.8% for a very heavy load, it is clear that the stretching of fibre, figure 2.4, is negligible during the forming process.

$$d(A,B) < d(A,C)$$

Figure 2.4 Illustration of the stretching of fibre

2.5.2 De-undulation of the fibre

In the fabric, the fibres are originally undulated. In the forming process, the fibres become tighter and the fabric looses its weaving regularity, figure 2.5. The de-undulation of fibre is also negligible.

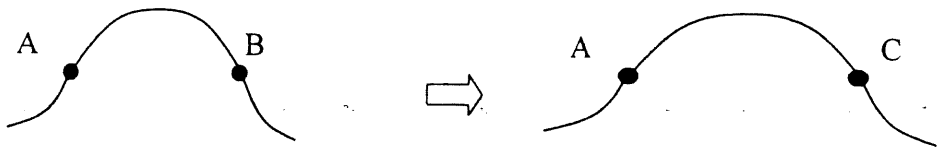

Figure 2.5 Illustration of the de-undulation of fibre

2.5.3 Sliding by shear of fibre

The mesh of the fabric is a more or less rigid set. When we pull on a corner of fabric, if the mesh can deform without changing the angle of its corner this phenomenon is called the sliding of the fibres, figure 2.6. Sliding is a undesirable characteristic.

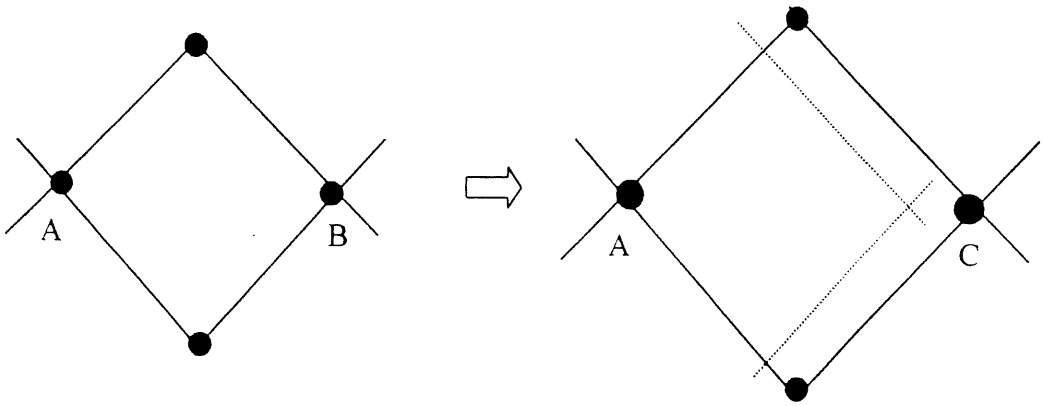

Figure 2.6 Illustration of sliding by shearing of fibres

In the reference [17] a kinematic model of fabric was presented. The experimental results have conducted to an empirical equation in which a corrective factor ''s'', featuring for the elongation of the elementary mesh and the angle θ between the warp and the weft, was introduced.

$$p = p_0\left(1 + s(1 - \frac{\theta}{90})\right) \qquad (2.1)$$

Where

p_0 : the length between the adjacent meshes of a non-deformed fabric

p : the length between the adjacent meshes of a deformed fabric

s : corrective factor

θ : angle between the warp and the weft

2.5.4 Deformation due to the trellis effect

During the forming process, the fibres are not stretched but they only change their directions, figure 2.7. That process needs less effort to obtain the large deformation. The small amount of energy needed for the trellis effect reinforces the fact that it is able to neglect the three previous types of deformation. It is also seen that this effect is close to what happens in the pure shearing of metal.

Finally, it can be assumed that the fibre deformations result exclusively from the trellis effect. The deformation of fabric is then reduced to simulate a geometrical problem – calculating the reorientation of fibres. In this model, the fabric constitutes of two families of unstretchable fibres which connect together by the rotating joints.

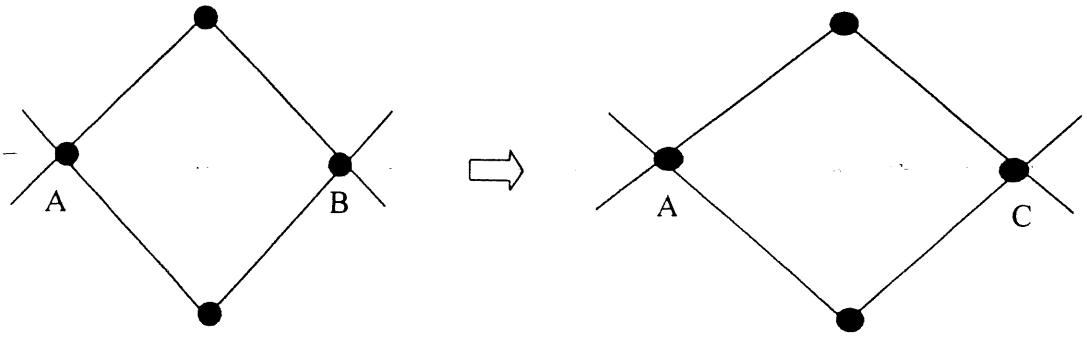

Figure 2.7 Illustration of the trellis effect

Generally, the numeric resolution for predicting the deformation of fabric during forming process can be realised by two ways:

- The algorithm based on the principle of minimisation of the elastic energy [18].
- The algorithm using the method of fisherman's net [19,20].

The minimisation of the elastic energy provides the results which are similar to ones obtained by the fisherman's net. However, the fisherman's net method is easier to use and gives a smaller error. Therefore, it will be used to predict the reorientation of fabric.

2.6 Deformations of the stratified composites during moulding

Laminate experiences a complex change in shape during the forming process due to external forces, die geometry, stacking sequence of fabric, etc. The forces, applied on material in which it deforms according to the form of the mould, play an important role on the microstructure of composite. The visco-elastic deformations occurring during the forming process, will affect strongly the mechanical performance of the specimen. Generally, the elastic behaviour of fibre structure and viscous behaviour of resin will influence the deformation of composite during the forming process.

For laminated composites, the deformation may be described in terms of five distinct possible mechanisms [21,22], illustrated in figure 2.8: resin percolation, longitudinal fibre flow, transverse fibre flow, in-plane shearing and interlaminar slip.

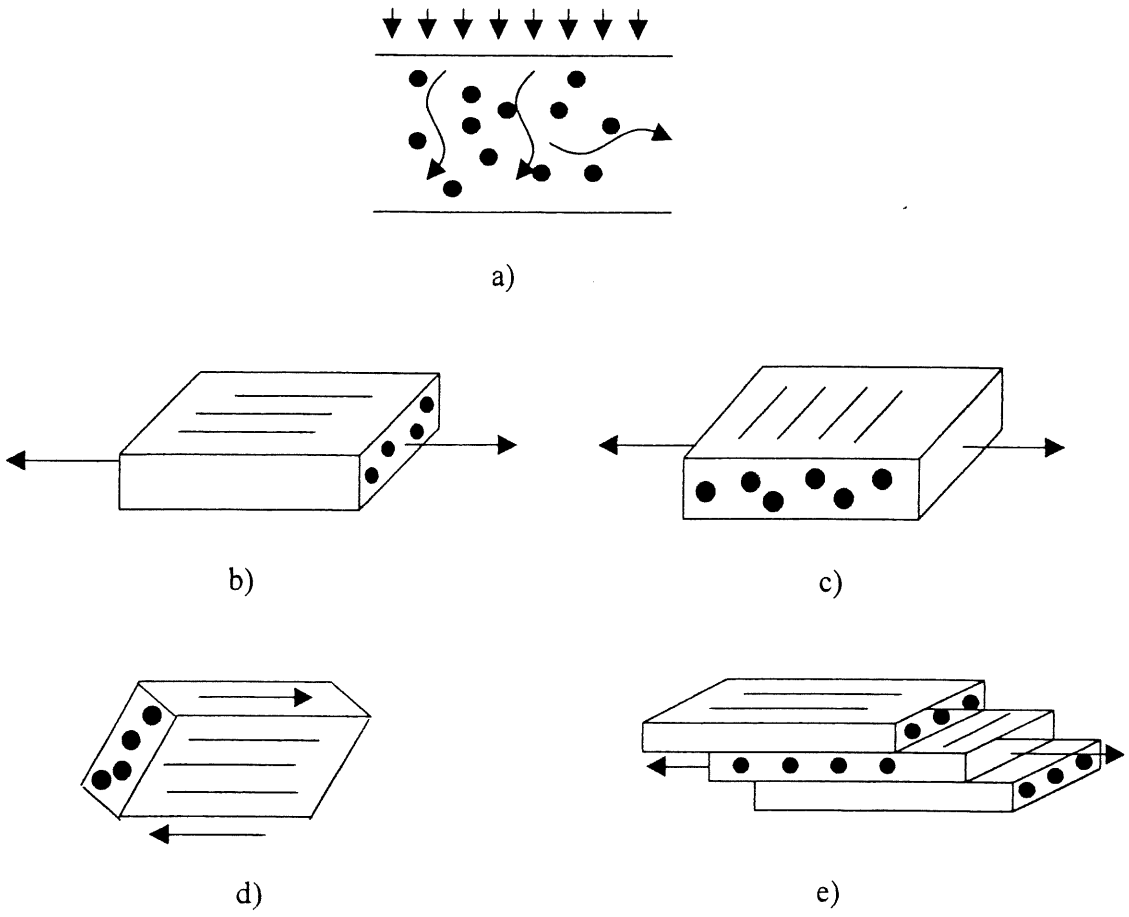

Figure 2.8 Fundamental deformation mechanisms involved in the forming of composite laminates: (a) resin percolation; (b) longitudinal fibre flow; (c) transverse fibre flow; (d) in-plane shearing; (e) interlaminar slip.

2.7 Kinematic model in the thickness sense

The forming process of fabric on a complex die geometry produces rearrangement of fibres, not only in the plan of fabric, but also in the thickness sense. In the fabric plan, the

deformation is supposed to be conformable to trellis effect, and modelised by the fisherman's net. In the thickness sense, two study cases must be distinguished, figure 2.9.

- Moulding with simple tool plate.
- Moulding with double tool plate.

a) b)

Figure 2.9 Illustration of two types of moulding: a) Moulding with simple tool plate, b) Moulding with double tool plate.

Since the specimens used in this research were fabricated by hand-lay-up method (the moulding with simple tool plate). This kind of moulding does not impose a uniform thickness to the fabric. The rearrangement of the fibre is assumed to be mainly governed by the trellis effect.

It means that for a laminate, the deformation mechanism can be represented by the figure 2.10.

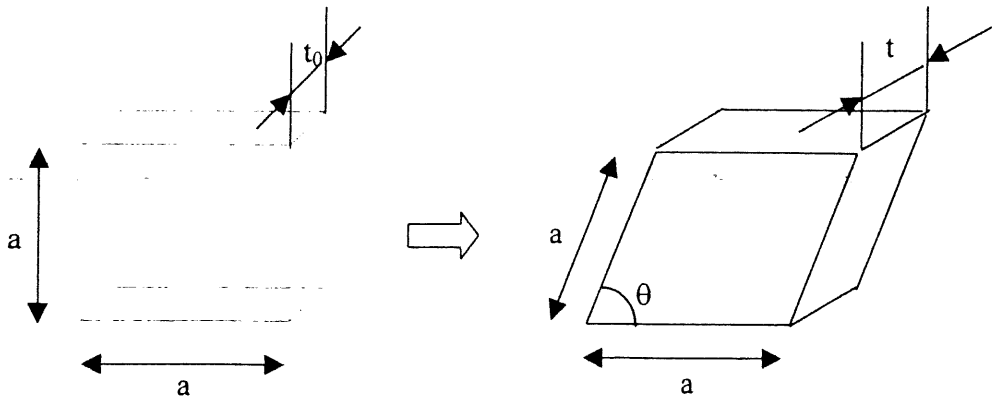

Figure 2.10 Modification of thickness under the forming process

It can be seen that the elementary mesh area is reduced due to the variation of angle θ. ($a^2 sin(\theta)$ instead of a^2). However, it has been assumed reasonably [23] that although ply thickness changes occur during forming, the local volume fraction doesn't change. The mathematical constraint derived from this assumption is that the thickness must be varied by the following law.

$$t = \frac{t_0}{\sin(\theta)} \qquad (2.2)$$

Furthermore, the hypothese of the fibre volume fraction staying constant implies that the engineering constant such as E_x, E_y, ν_{xy}, G_{xy} are independent of the angle θ.

2.8 Residual stress

It is known that the existence of residual stress can cause micro cracking in resin matrix, warping, buckling and the difference in shape between the mould and fabricated piece. Since the residual stress has a significant influence in the prediction of the mechanical behaviour as well as the longevity of fabricated piece, a serie of publications [24,25,26] has contributed to the research on its effect on composite material.

We distinguish that there exist two types of residual stress with a thermoset matrix. One derives from the thermal strain and the other links to the chemical shrinkage of resin. At the beginning of the fabrication cycle, most of chemical shrinkage takes place, induced by the cross-link. The residual stress derived from the thermal strain are the following.

- The non-uniform variation due to the change of temperature inside the piece.
- The deformations of the piece is limited in certain points by boundary conditions.
- The anisotropy of the material.

The fabrication process follows the strictly technical requirements in order to avoid the first two types of residual stresses. Consequently, these two types of stresses appear as the result of fabrication or manipulation error.

The anisotropy of material is then the principal phenomena that induces the residual stresses. It is high enough to cause the cracks even before any load is applied [27]. From an analytical point of view, these residual stresses have been modelled on a basis of elastic behaviour material [24].

To simplify the calculation process, the thermo-mechanic behaviour is supposed to be linear during the process of fabrication by Hahn and Pagano [24]. That means the coefficients of tensor of rigidity and thermal expansion are constant. This assumption is still valid in condition that the magnitude of resin shrinkage in the mould is known.

The residual stresses σ_i^R have been modelled [28] by the following formula, which σ_i^R is a linear function of the temperature.

$$\sigma_i^R = Q_{ij}\left(\varepsilon_j^0 + zk_j - \varepsilon_j^R\right) \qquad (2.3)$$

Where:

σ_i^R : residual stress

Q_{ij} : tensor of rigidity

ε_j^0 : strain component in mid-plane

z : coordinate in thickness direction

k_j : curvature

ε_j^R: strain caused by thermal and chemical shrinkage

2.8.1 Stiffness of laminates

The mechanical behaviour of a laminate is the superposition of the mechanical properties of each unidirectional ply. We can apply the Hooke's law to evaluate the stiffness of unidirectional ply. Since composite material is anisotropic, it is important to distinguish the difference between two material coordinate systems: The on-axis system and the off-axis system. In the on-axis system, the x-axis is along with the fibre direction, figure 2.11, while in the off-axis system, the x-axis rotates about the fibre direction through an angle θ, which is called the skew angle. The relation between stress σ_i and strain ε_i on the on-axis system of one unidirectional ply is the following.

$$\begin{bmatrix} \sigma_x \\ \sigma_y \\ \sigma_s \end{bmatrix} = \begin{bmatrix} Q_{xx} & Q_{xy} & 0 \\ Q_{xy} & Q_{yy} & 0 \\ 0 & 0 & Q_{ss} \end{bmatrix} \cdot \begin{bmatrix} \varepsilon_x \\ \varepsilon_y \\ \varepsilon_s \end{bmatrix} \qquad (2.4)$$

The stiffness coefficients Q_{ij} can be determined directly from the engineering constant.

$$\begin{aligned} Q_{xx} &= mE_x \\ Q_{xy} &= mE_y \\ Q_{yy} &= mE_y \\ Q_{ss} &= G_{xy} \end{aligned} \qquad (2.5)$$

where

$$m = \frac{1}{\left[1 - \frac{\nu_{xy}^2 E_y}{E_x}\right]}$$

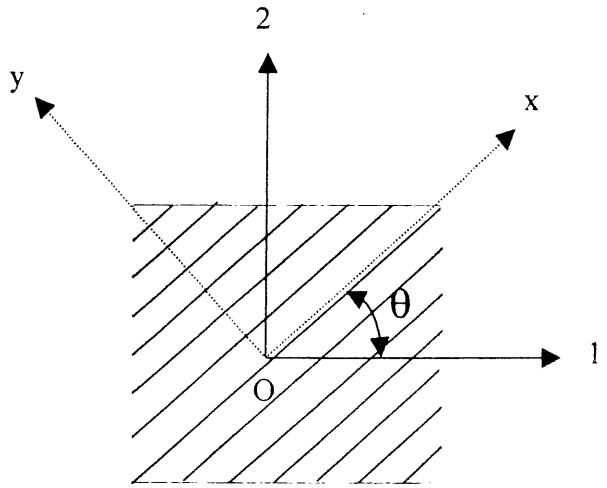

Figure 2.11 The coordinate system for a unidirectional ply. Oxy: on-axis system, O12 : off-axis system.

Using the transformation matrix [28], the relation between the stress and strain in the off-axis system of a unidirectional ply can be expressed as

$$\begin{bmatrix} \sigma_1 \\ \sigma_2 \\ \sigma_6 \end{bmatrix} = \begin{bmatrix} Q_{11} & Q_{12} & Q_{16} \\ Q_{12} & Q_{22} & Q_{26} \\ Q_{16} & Q_{26} & Q_{66} \end{bmatrix} \cdot \begin{bmatrix} \varepsilon_1 \\ \varepsilon_2 \\ \varepsilon_6 \end{bmatrix} \qquad (2.6)$$

where

$$
\begin{aligned}
Q_{11} &= Q_{xx}\cos^4\theta + Q_{yy}\sin^4\theta + 2(Q_{xy} + 2Q_{ss})\sin^2\theta\cos^2\theta \\
Q_{22} &= Q_{xx}\sin^4\theta + Q_{yy}\cos^4\theta + 2(Q_{xy} + 2Q_{ss})\sin^2\theta\cos^2\theta \\
Q_{12} &= (Q_{xx} + Q_{yy} - 4Q_{ss})\sin^2\theta\cos^2\theta + Q_{xy}(\cos^4\theta + \sin^4\theta) \\
Q_{66} &= (Q_{xx} + Q_{yy} - 2Q_{xy} - 2Q_{ss})\sin^2\theta\cos^2\theta + Q_{ss}(\cos^4\theta + \sin^4\theta) \\
Q_{16} &= (Q_{xx} - Q_{xy} - 2Q_{ss})\sin\theta\cos^3\theta - (Q_{yy} - Q_{xy} - 2Q_{ss})\sin^3\theta\cos\theta \\
Q_{26} &= (Q_{xx} - Q_{xy} - 2Q_{ss})\sin^3\theta\cos\theta - (Q_{yy} - Q_{xy} - 2Q_{ss})\sin\theta\cos^3\theta
\end{aligned}
\tag{2.7}
$$

Finally, the stress resultant N_i and moment M_i of a laminate can be expressed as functions of the deformation ε_j^0 of the neutral fibre and the curvature k_j.

$$
\begin{Bmatrix} N_i \\ M_i \end{Bmatrix} = \begin{bmatrix} A_{ij} & B_{ij} \\ B_{ij} & D_{ij} \end{bmatrix} \cdot \begin{Bmatrix} \varepsilon_j^0 \\ k_j \end{Bmatrix} \tag{2.8}
$$

where

$$
\begin{aligned}
A_{ij} &= \int Q_{ij}\,dz \\
B_{ij} &= \int Q_{ij}\,z\,dz \\
D_{ij} &= \int Q_{ij}\,z^2\,dz
\end{aligned}
\tag{2.9}
$$

2.9 Woven fabric composite model

Polymer reinforced by woven fabrics are probably the most commonly used composites in structural applications such as aircraft, boats, reservoirs, pressure vessels, etc. Woven fabric offers many advantages in terms of manipulative requirements, including dimensional stability, good conformability, and deep-draw shape ability. Moreover, compared to unwoven unidirectional composites, the woven–fabric composites provide more balanced properties, higher impact resistance, easier handling and lower fabrication cost, particularly for parts with complex shapes. Deliberate efforts have been made to model the thermo-mechanical

performance of woven fabric composites. The various mathematical models have been developed by considering the actual properties and all possible parameters that might affect the results. Up to now, four main workable models are known as the mosaic model, the fibre undulation model (crimp model), the bridging model, and the sub-plies model.

2.9.1 Mosaic model

In the mosaic model, proposed by Chou [29], the woven composite is idealized by an assembly of cross-ply laminates [0/90] in series, figure 2.12. The stiffness coefficients of the mosaic model are evaluated by using the classical laminate theory.

With a simple structure, the mosaic is unable to take into account the stress perturbation, the deformation as well as the continuity of fibre inside laminates in the undulated zone.

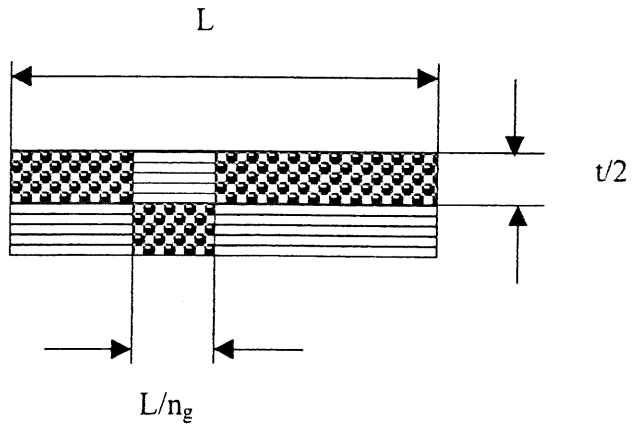

Figure 2.12 Modelisation of mosaic model

In this model, the stiffness coefficients $\overline{A}_{ij}$, $\overline{B}_{ij}$ and $\overline{D}_{ij}$ of a certain woven composite can be calculated by a cross-ply laminate with the same thickness and fibre volume fraction as the woven fabric.

$$\overline{A}_{ij} = A_{ij}$$
$$\overline{B}_{ij} = \left(1 - \frac{2}{n_g}\right) B_{ij} \qquad (2.10)$$
$$\overline{D}_{ij} = D_{ij}$$

Although the mosaic model appears to be easy to use, it can't be applied for the fabric which is no longer orthogonal.

2.9.2 Fibre undulation model

The fibre undulation model [30] is developed to consider the continuity and the undulation of fibre in fabric composites. This model, illustrated in figure 2.13, permits to determinate the stress behaviour and the deformation of woven composite in the undulated zone. The undulated zone is depicted by three geometrical parameters $h_1(x)$, $h_2(x)$, and a_u which are shown in figure 2.13 The fibre undulation model is applicable to n_g values in general. However, it is only effective for characterizing the plain weave and seems to be less effective for the satin where $n_g \geq 4$.

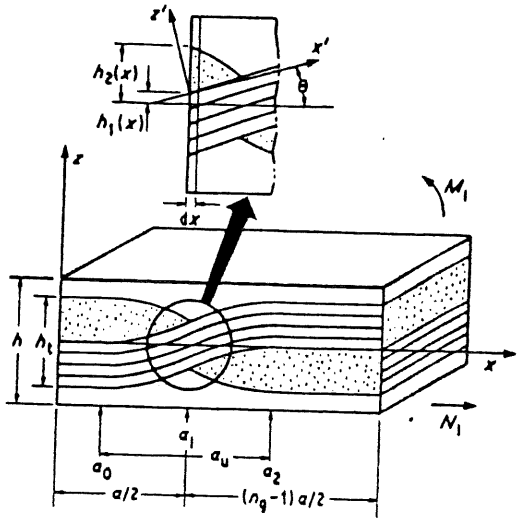

Figure 2.13 Modelisation of the fibre undulation model

2.9.3 Bridging model

This model [31] utilises the concept of two previous models. It is valid for only satin weave where $n_g \geq 4$. Figure 2.14 represents a basis interlaced region in the satin weave called the repeating unit. A schematic view of the bridging model is shown in figure 2.14 c for a repeating unit, which consists of the interlaced region and its surrounding areas. The four regions labelled by A, B, D and E consist of straight fill threads, and hence can be regarded as pieces of cross-ply laminates. Region C has an interlaced structure with an undulated fill thread. In this model, the regions B and D carry higher loads than region C and act as bridges for load transfer between regions A and E. For plain weave fabric, since there are no straight thread regions surrounding an interlaced region, the bridge model is no longer valid.

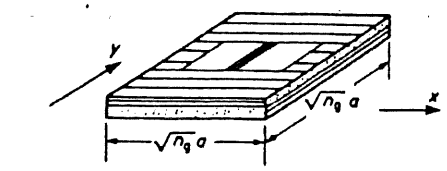

a)

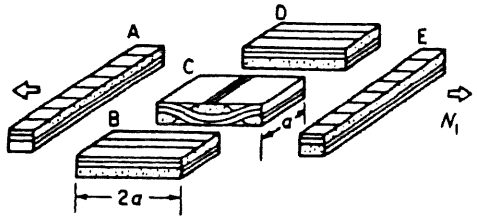

b)

Figure 2.14 Modelisaion of the bridging model. a) Repeating unit, b) Decompostion of model

2.9.4 Sub-plies model

In the sub-plies model [32], the fabric is considered as a laminate consisting of four fictional unwoven unidirectional plies, figure 2.15. The fibre orientation of these four fictional plies is arranged as an anti-symmetric structure that can be considered generally as [θ/-θ/θ/-θ].

It has been shown in [32] that the fictional thickness e can be expressed as a function of the fabric thickness t_0 and n_g.

$$e = t_0\sqrt{\frac{1}{n_g}} \qquad (2.11)$$

Where n_g is a geometrical parameter which presents a wrap thread interlacing with n_g fill threads. The stiffness coefficients of this laminate A_{ij}^s, B_{ij}^s, and D_{ij}^s can be obtained from the classical laminate theory.

$$
\begin{aligned}
A_{ij}^S &= A_{ij} \\
B_{ij}^S &= \left(1 - \frac{2}{n_g}\right) B_{ij} \\
D_{ij}^S &= D_{ij}
\end{aligned}
\tag{2.12}
$$

where A_{ij}, B_{ij} and D_{ij} are the stiffness coefficients of a [0/90] cross-ply laminate with the same fibre volume fraction and total thickness as that of the fabric composite.

Sub-plies model is identified with the shell element in any finite element code. Therefore, it is able to use directly its engineering constants in finite element code without any transferring procedure.

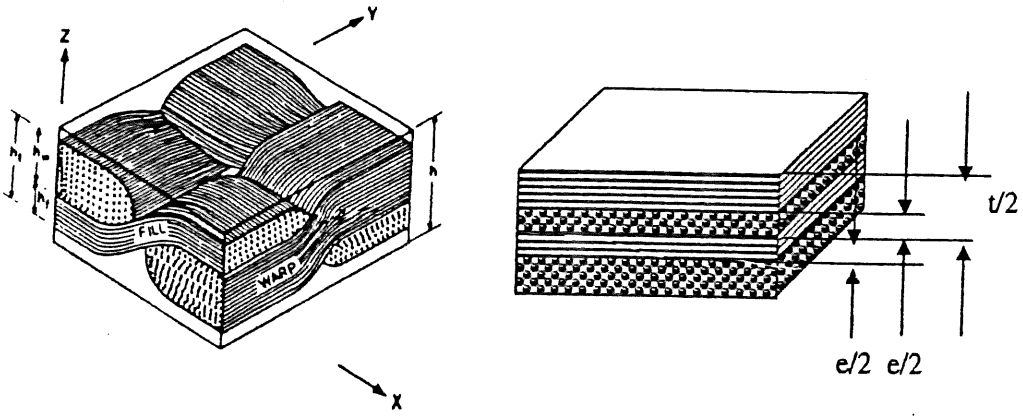

Figure 2.15 Modelisation of the sub-plies model

2.10 Effect of non-linear on the after curing shape of unsymmetric laminates

It is well known that the unsymmetric laminates experience a change in shape after curing due to the existence of residual stress. Classical lamination theory predicts the after curing shape of all unsymmetric laminates to be saddle, figure 2.16. Experimental observations, however, indicate that some unsymmetric laminates have cylindrical shape. Moreover, the out-of-plane deformation is many time higher than the thickness (geometrical non-linear). For composites made of polyester with room-temperature curing and high level of shrinkage, the same phenomena occurs on thin unsymmetric laminate.

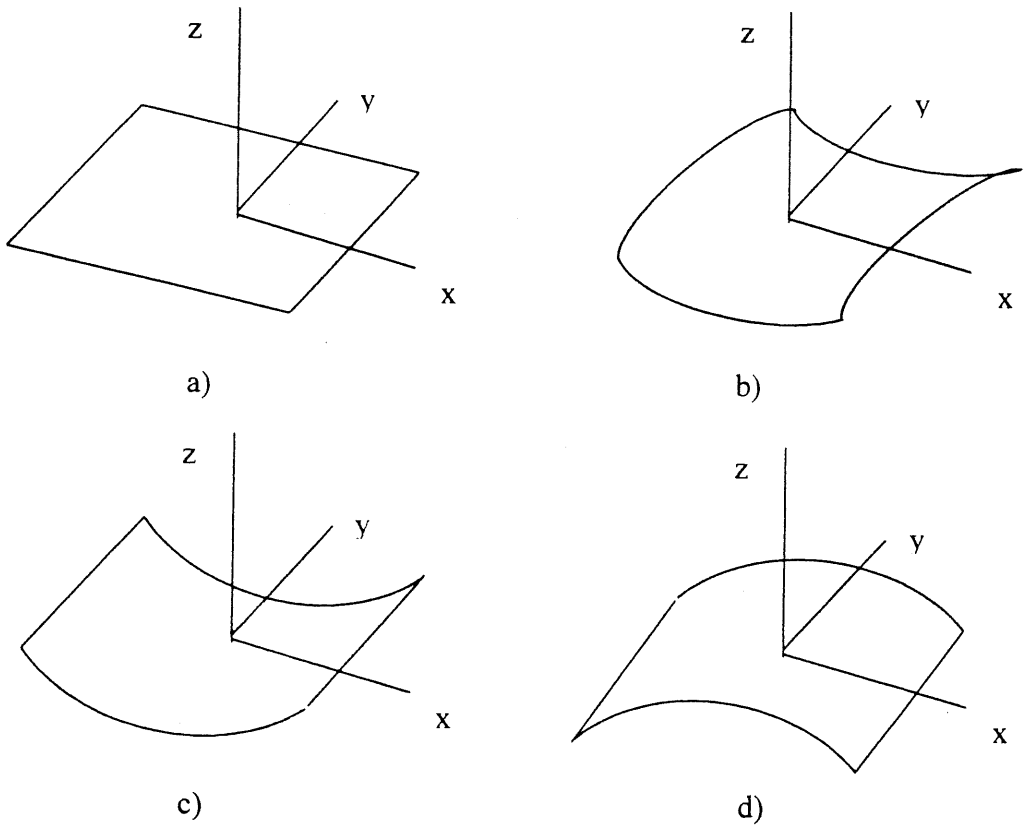

Figure 2.16 Laminate shapes: a) room-temperature, b) a saddle shape, c) a cylindrical shape, d) another cylindrical shape.

CHAPTER III

METHODOLOGY

3. METHODOLOGY

3.1 Summary description

This chapter presents the methodology to predict the complex arrangement of fabric during the forming process as well as its effect on strain and residual stress. The chapter will thus be divided into three main parts.

The first part will focus on the determination of the stiffness coefficients of woven fabric composite. In this part, the woven fabric composite will be modelled using the sub-plies model. The effect of fibre's undulation will be taken into account through the test data.

The second part describes the method to predict the shrinkage coefficients. The mechanical properties, determined from the first part, are utilised to evaluate the shrinkage coefficients. Two methods according to two kinds of sample: cross-ply and angle ply samples, will be presented. As to be seen for a composite fabricated from the unsymmetric woven fabric and the matrix with a high level of shrinkage, the non-linear effect on the deformation becomes significant. Therefore, the discussion on the non-linear method will be presented.

The last part is the synthesis of the two previous parts. The technique used for addressing the shrinkage of a complex geometrical piece after moulding will be presented. The fisherman's net method is used to predict the fibre's reorientation. The finite element method is then used to determine the strain and residual stress.

3.2 Material choice

The deformations appearing during the forming process depend on the fibre's structure of composite. In order to show the possible influences of the weaving type of fabric on modes of

deformation, two types of fabrics were utilised, plain weave and 8-harness satin. The first type is strongly affected by the fibre's undulation and easy to deform during moulding while the second type is less affected by the fibre's undulation and make it harder to follow the die geometry. The utilisation of these two types of fabrics permits a verification which, through it, we can assess the effects of the different intermediate types of fabrics on the deformation of woven composites. Therefore, in this work, *resin polyester* reinforced *by glass fibre woven in the plain weave and 8-harness satin patterns* was utilised.

3.3 Study form

The piece used to study the shrinkage in woven fabric composite must satisfy the following conditions.

- It must have the form which is often used in industry
- It is easy to fabricate
- It permits the existence of the possible deformed mechanisms of woven fabric such as longitudinal fibre flow, transverse fibre flow, in-plane shearing, and interlaminar slip, see paragraph 2.6.
- It permits to avoid the fibre kinking during the forming process.
- It is easy to remove from the mould after moulding

To satisfy the above demands, the chosen piece has the shape of a rounded cone. The rounded cone is modelled by a right circular cone in which the top of the cone has been replaced by a spherical shell, figure 3.1. The spherical sector is assumed to be joined smoothly to the cone by having the same diameter and the same slope of the cone at the junction.

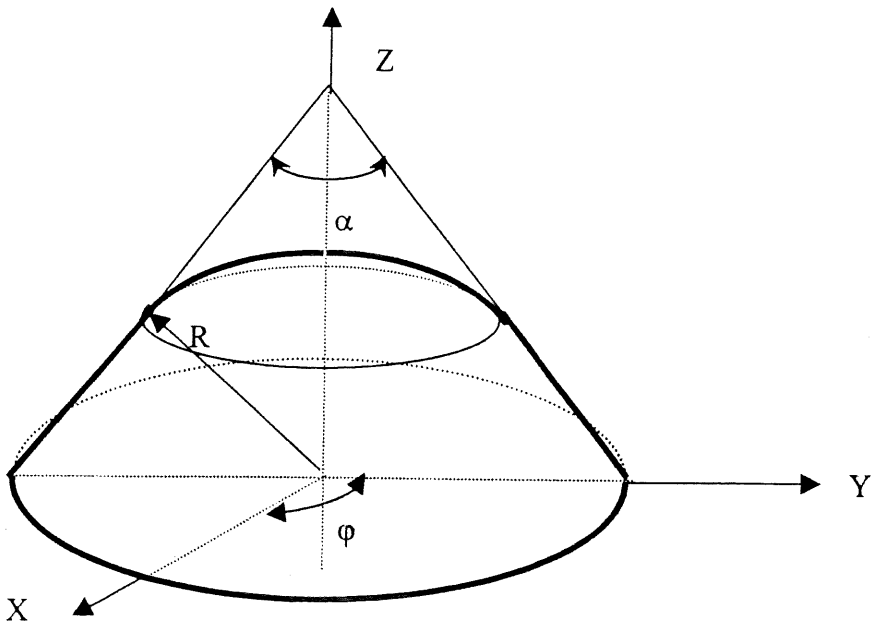

Figure 3.1 Rounded cone

The rounded cone belongs to the family of pieces which have the double curvature. This is the most popular form in many industrial applications. With such a three dimensional structure, the piece permits the existence of all admissible deformed mechanisms.

According to [20], the relation between the cone angle α and the minimum angle of fabric (the minimum angle between the weft and the warp) can be established by an empirical equation.

$$\theta_{min} = 90^0 \sin(\frac{\alpha}{2}) \qquad (3.1)$$

To avoid the fibre kinking, the minimum angle of fabric must be greater than 45^0.

On the analytical point of view, the dimension of piece does not affect the numerical results. However, the research from [17] demonstrated that a rounded cone with a hemispherical diameter <25.45mm will cause an important dispersion in numerical result.

In order to reduce the dispersion of the result, a radius of 60mm for the spherical sector and a height of 60mm for the rounded cone was chosen. Figure 3.2 illustrates the chosen geometrical dimensions.

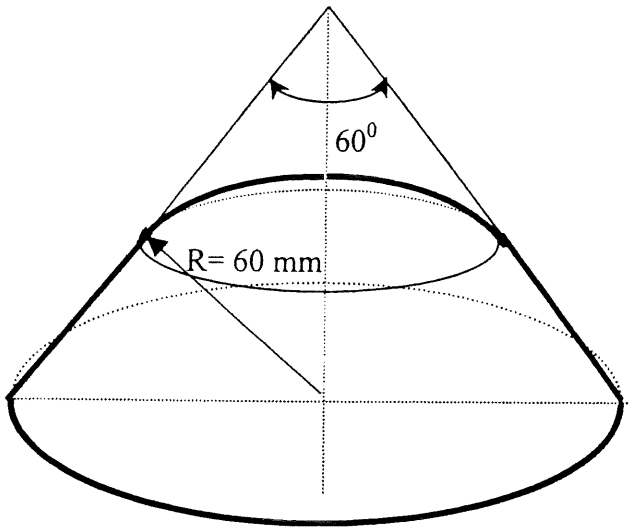

Figure 3.2 Dimensions of the chosen rounded cone.

3.4 Thermo-Elastic Properties of the Unidirectional Sub-plies

Since the fibre undulation is not considered in the sub-plies model, the prediction of thermo-elastic properties of fabric composite based on this one becomes less accurate. Especially, for fabric with a low value of n_g such as plain weave fabrics, the model may lead to significant error.

To make the stiffness coefficients of the model more appropriate, the properties of the unidirectional sub-plies should be modified in such a way that the effect of fibre undulation must be taken into account. These modified properties can be obtained through the

experimental measurement on moulded specimens made from the woven fabric composite. According to reference [32], two tension tests are necessary for such characterization : a $[(0/90)_n]_s$ test and a $[(+45/-45)_n]_s$ test, where the angles correspond to the yarn orientations in the fabric. The stiffness coefficients of the equivalent unidirectional sub-plies ($Q_{xx[eq]}$, $Q_{xy[eq]}$, $Q_{yy[eq]}$ and $Q_{ss[eq]}$), can thus be calculated from the Young's modulus and the Poisson's ratios of these tension tests.

From the tension tests on $[(0/90)_n]_s$ specimens, the Young's modulus $E_{[0/90]}$ and the Poisson's ratio $\nu_{[0\,90]}$ are given respectively by eqns (3.2) and (3.3) as a function of the stiffness coefficients of the equivalent unidirectional sub-plies.

$$E_{[0\ 90]} = \frac{Q_{xx[eq]} + Q_{yy[eq]}}{2} - \frac{2Q_{xy[eq]}^2}{Q_{xx[eq]} + Q_{yy[eq]}} \tag{3.2}$$

$$\nu_{[0/90]} = \frac{2Q_{xy[eq]}}{Q_{xx[eq]} + Q_{yy[eq]}} \tag{3.3}$$

These equations can be combined to obtain the stiffness coefficient of the equivalent unidirectional sub-plies $Q_{xy[eq]}$.

$$Q_{xy[eq]} = \frac{E_{[0\ 90]}\nu_{[0/90]}}{1 - \nu_{[0/90]}^2} \tag{3.4}$$

Similarly, the sum of the stiffness coefficients $Q_{xx[eq]}$ and $Q_{yy[eq]}$ can be expressed as

$$Q_{xx[eq]} + Q_{yy[eq]} = \frac{2E_{[0\ 90]}}{1 - \nu_{[0,90]}^2} \tag{3.5}$$

Generally, we can not separate these two coefficients from test data of tension test. However, it is reasonable to assume that the fibre undulation does not have a significant effect on the transverse Young's modulus. Therefore, the transverse modulus of the equivalent unidirectional composite $E_{y[eq]}$ of sub-plies model could be considered equal to the transverse modulus of unidirectional composite $E_{y[unidir]}$. The relation is then given by

$$E_{y[eq]} = E_{y[unidir]} = Q_{yy[eq]} - \frac{Q_{xy[eq]}^2}{Q_{xx[eq]}} \tag{3.6}$$

By combining eqns (3.4), (3.5) and (3.6), eqn (3.7) can be obtained. The stiffness coefficient $Q_{xx[eq]}$ can be deduced by solving this equation.

$$Q_{xx[eq]}^2 + \left(E_{y[unidir} - \frac{2E_{[0\ 90]}}{1 - \nu_{[0\ 90]}^2} \right) Q_{xx[eq]} + Q_{xx[eq]}^2 = 0 \tag{3.7}$$

Substituting the values of $Q_{xx[eq]}$ and $Q_{xy[eq]}$ into eqn (3.6), we can obtain the stiffness coefficient $Q_{yy[eq]}$.

From the tension test on $[(+45/-45)_n]_s$, the Young's modulus ($E_{[+45/-45]}$) and the Poisson's ratio ($\nu_{[+45/-45]}$) can be expressed as a function of the stiffness coefficients of the equivalent unidirectional sub-ply.

$$\begin{aligned} E_{[45\ -45]} &= \frac{4Q_{ss[eq]}(Q_{xx[eq]} + Q_{yy[eq]} + 2Q_{xy[eq]})}{Q_{xx[eq]} + Q_{yy[eq]} + 2Q_{xy[eq]} + 4Q_{ss[eq]}} \\ \nu_{[45\ -45]} &= \frac{Q_{xx[eq]} + Q_{yy[eq]} + 2Q_{xy[eq]} - 4Q_{ss[eq]}}{Q_{xx[eq]} + Q_{yy[eq]} + 2Q_{xy[eq]} + 4Q_{ss[eq]}} \end{aligned} \tag{3.8}$$

Similarly to the case of $[(0/90)_n]_s$ tension test, eqn (3.8) can be combined to obtain the stiffness coefficient of the equivalent unidirectional composite $Q_{ss[eq]}$.

$$Q_{ss[eq]} = \frac{E_{[+45/-45]}}{2(1 + \nu_{[+45/-45]})} \tag{3.9}$$

3.5 Characterization of equivalent on-axis shrinkage coefficients

The equivalent on-axis shrinkage coefficients $\gamma_{x[eq]}$ and $\gamma_{y[eq]}$ can be calculated in the same manner of thermal expansion coefficients. Generally, the shrinkage coefficients can be determined by two kinds of sample: using the $[0/90]_n$ or $[+\theta/-\theta]_n$ woven fabric. With laminates fabricated from plain weave which have zero curvature after moulding, the $[+\theta/-\theta]_n$

samples supply a simple procedure for evaluating the shrinkage coefficients. While the laminates fabricated from satin such as 8-harness satin can use both kinds of sample as well. On the other hand, the out-of-plane deformation due to the chemical shrinkage in polyester reinforced by unsymmetric woven fabric, for instance 8-harness satin, seems to be governed by the non-linear rule rather than the linear one. Therefore, without loss of generality, the formulas for calculating shrinkage coefficients will be presented in two ways: using classical laminate theory and non-linear extension.

3.5.1 Determination of the shrinkage coefficients by cross-ply laminate $[0/90]_n$

As mentioned above, the thermal expansion coefficients can be replaced by the shrinkage coefficients. According to the reference [33], the in-plane strain ε_i and curvature K_i can be written as functions of on-axis ply stiffness and shrinkage coefficients.

$$K_1 = \frac{24Q_3}{t_0}\frac{1}{m}\left(1-\frac{2}{n_g}\right)\times\frac{\gamma_{y[eq]}-\gamma_{x[eq]}}{4(Q_1+Q_2+4Q_3)-3(Q_1+Q_2)\left(1-\frac{2}{n_g}\right)^2\frac{1}{m^2}}$$

$$K_2 = -K_1 \qquad (3.10)$$

$$K_6 = 0$$

and

$$\varepsilon_1 = \frac{\left[4(Q_1+2Q_3)-3(1-\frac{2}{n_g})^2\frac{Q_1}{m^2}\right]\gamma_x+\left[4(Q_2+2Q_3)-3(1-\frac{2}{n_n})^2\frac{Q_2}{m^2}\right]\gamma_y}{4(Q_1+Q_2+4Q_3)-3(Q_1+Q_2)\left(1-\frac{2}{n_g}\right)^2\frac{1}{m^2}}$$

$$\varepsilon = \varepsilon_1 \qquad (3.11)$$

$$\varepsilon_6 = 0$$

where

$$Q_1 = (Q_{xx[eq]}-Q_{yy[eq]})(Q_{xx[eq]}-Q_{xy[eq]})$$

$$Q_2 = (Q_{xx[eq]}-Q_{yy[eq]})(Q_{xy[eq]}-Q_{yy[eq]}) \qquad (3.12)$$

$$Q_3 = Q_{xx[eq]}Q_{yy[eq]} - Q^2_{xy[eq]}$$

The on-axis equivalent shrinkage coefficients $\gamma_{x[eq]}$ and $\gamma_{y[eq]}$ can be solved from eqns (3.10) and (3.11), i.e.

$$\gamma_{x[eq]} = \frac{c(a_3\varepsilon_1' - a_2 K_1)}{a_3(a_1 + a_2)} \qquad (3.13)$$

$$\gamma_{y[eq]} = \frac{c(a_3\varepsilon_1' + a_1 K_1)}{a_3(a_1 + a_2)} \qquad (3.14)$$

where

$$a_1 = 4(Q_{xx[eq]} + Q_{yy[eq]} - 2Q_{xy[eq]})(Q_{xx[eq]} + Q_{xy[eq]})$$
$$-3(1-\frac{2}{n_g})^2 \frac{1}{m^2}(Q_{xx[eq]} - Q_{yy[eq]})(Q_{xx[eq]} - Q_{xy[eq]})$$
$$a_2 = 4(Q_{xx[eq]} + Q_{yy[eq]} - 2Q_{xy[eq]})(Q_{xy[eq]} + Q_{xy[eq]})$$
$$-3(1-\frac{2}{n_g})^2 \frac{1}{m^2}(Q_{xx[eq]} - Q_{yy[eq]})(Q_{xy[eq]} - Q_{yy[eq]}) \qquad (3.15)$$
$$a_3 = \frac{24}{tm}\left(1-\frac{2}{n_g}\right)\left(Q_{xx[eq]}Q_{yy[eq]} - Q^2_{xy[eq]}\right)$$
$$c = 4[(Q_{xx[eq]} - Q_{yy[eq]})^2 + 4Q_{xx[eq]}Q_{yy[eq]} - 4Q^2_{xy[eq]}]$$
$$-3\left(1-\frac{2}{n_g}\right)^2 \frac{1}{m^2}(Q_{xx[eq]} - Q_{yy[eq]})^2$$

3.5.2 Determination of the shrinkage coefficients by angle-ply laminate $[\theta/-\theta]_n$

From the classical laminate theory [28], the in-plane strain ε_i can be written as function of resultant force F_i and stiffness of angle-ply laminate A^S_{ij}, B^S_{ij}, D^S_{ij}

$$\varepsilon_1 = \frac{A^S_{22}(N_1 - B^S_{16}k_6) - A^S_{12}(N_2 - B^S_{26}k_6)}{A^S_{12}A^S_{22} - (A^S_{12})^2}$$
$$\varepsilon_2 = \frac{A^S_{11}(N_2 - B^S_{26}k_6) - A^S_{12}(N_1 - B^S_{16}k_6)}{A^S_{12}A^S_{22} - (A^S_{12})^2} \qquad (3.16)$$

where

$$N_1 = ph + qh\cos(2\theta)$$
$$N_2 = ph - qh\cos(2\theta) \qquad (3.17)$$
$$k_6 = \frac{h^2}{4D^S_{66}} p\sin(2\theta)$$

A^S_{ij}, B^S_{ij}, D^S_{ij}: determined from eqn (2.7).(2.9) and (2.12)

θ: skew angle

$$p = \frac{1}{2}(Q_{xx[eq]} + Q_{xy[eq]})\gamma_{xx[eq]} + \frac{1}{2}(Q_{xy[eq]} + Q_{yy[eq]})\gamma_{yy[eq]}$$
$$q = \frac{1}{2}(Q_{xx[eq]} - Q_{xy[eq]})\gamma_{xx[eq]} + \frac{1}{2}(Q_{xy[eq]} - Q_{yy[eq]})\gamma_{yy[eq]} \qquad (3.18)$$

Two unknowns p, q can be solved by substituting the experimental values of ε_i and eqn (3.17) into eqn (3.16). Once p, q are determined the shrinkage coefficients can be calculated from eqn (3.18). i.e.

$$\gamma_x = \frac{q(Q_{xy} + Q_{yy}) + p(Q_{yy} - Q_{xy})}{Q_{xx}Q_{yy} - Q^2_{xy}} \qquad (3.19)$$

$$\gamma_y = \frac{p(Q_{xx} - Q_{xy}) - q(Q_{xx} + Q_{xy})}{Q_{xx}Q_{yy} - Q^2_{xy}} \qquad (3.20)$$

3.6 Non-linear expansion

For non-linear theory, it was assumed that the out-of-plane displacement of unsymmetric laminates is many times the laminate thickness. Accordingly, the Von Karman approximation to Green's strain should be used. The strain-displacement relations are as follows:

$$\begin{aligned}
\varepsilon_{xx} &= \frac{\partial u^2}{\partial x} - z\frac{\partial^2 w}{\partial x^2} + \frac{1}{2}\left(\frac{\partial w}{\partial x}\right)^2 \\
\varepsilon_{yy} &= \frac{\partial v^0}{\partial y} - z\frac{\partial^2 w}{\partial y^2} + \frac{1}{2}\left(\frac{\partial w}{\partial y}\right)^2 \\
\varepsilon_{xy} &= \frac{1}{2}\left[\frac{\partial u^0}{\partial y} + \frac{\partial v^0}{\partial x} - 2z\frac{\partial^2 w}{\partial x \partial y} + \frac{\partial w}{\partial x}\frac{\partial w}{\partial y}\right]
\end{aligned} \tag{3.21}$$

For the cross-ply laminate, the out-of-plane deformation are assumed:

$$w = \frac{1}{2}(a_0 x^2 + b_0 y^2) \tag{3.22}$$

The mid-plane displacements of the laminate are assumed to be of the following form [14]:

$$\begin{aligned}
u^0 &= a_1 x - \frac{a^2}{6}x^3 + a_2 x y^2 \\
v^0 &= b_1 y - \frac{b^2}{6}y^3 + b_2 x^2 y
\end{aligned} \tag{3.23}$$

Eqn (3.22) and eqn (3.23) are substituted subsequently into eqn (3.21), the mid-plane strains are expressed as:

$$\begin{aligned}
\varepsilon^0_{xx} &= a_1 + a_2 y^2 \\
\varepsilon^0_{yy} &= b_1 + b_2 x^2 \\
\varepsilon^0_{xy} &= (a_2 + b_2 + \frac{a_0 b_0}{2})xy
\end{aligned} \tag{3.24}$$

If the restriction that $\varepsilon^0_{xy}=0$, i.e $a_2=b_2= -a_0b_0/4$ are applied in eqn (3.24) and then the mid-plane strains in eqn (3.24) turn into the Hyer's formulation [12].

3.6.1 Minimal potential energy

It is reasonable to assume that the external load is not important during the shrinkage process. Thus, the potential energy, including the effects of shrinkage expansion, is written as:

$$W = \int_V \Omega dV \tag{3.25}$$

where

$$\Omega = \frac{1}{2} C_{ij} (\varepsilon_i \varepsilon_j - \gamma_i \varepsilon_j) \tag{3.26}$$

After the strain energy density function is expanded in a power series, where ε_{ij} are small and terms higher than the second order are neglected, the reduced tensor form of the potential energy is:

$$W = \frac{1}{2} \overline{Q}_{ij} \varepsilon_i \varepsilon_j - \gamma_i \varepsilon_j \tag{3.27}$$

Where $\overline{Q}_{ij}$ denotes the reduced transformed stiffness and γ_i are shrinkage coefficients.

As can be seen, the potential energy can be expressed in terms of a_i, b_i, x, y, z, $\overline{Q}_{ij}$ and γ_i:

$$W = \int_x \int_y \int_z \Omega(a_i, b_i, x, y, z, \overline{Q}_{ij}, \gamma_i) dx dy dz \tag{3.28}$$

The first variation of W must be zero to satisfy the condition of equilibrium of energy, i.e.

$$\delta W = \sum \left(\frac{\partial W}{\partial a_i} \right) \delta a_i + \sum \left(\frac{\partial W}{\partial b_i} \right) \delta b_i = 0 \qquad (3.29)$$

Where i=0,1: neglect the in-plane shear strain; i=0,1,2: assume the in-plane shear strain.

Eqn (3.29) leads to the condition that each of partial variation must be zero. Therefore

$$\begin{aligned} \frac{\partial W}{\partial a_i} &= 0 \\ \frac{\partial W}{\partial b_i} &= 0 \end{aligned} \qquad (3.30)$$

With the assumption of in-plane shear strain or not, the above equations result in six or four non-linear simultaneous equations. The coefficients, a_i, b_i, that were deduced from these equations are used to construct mid-plane strains. Furthermore, in order to minimize the energy, $\delta^2 W$ must be positive and definite. A non-linear Newton-Raphson iteration is used to calculate numerically $\delta^2 W$. See appendix A for the detail of system of equations (3.30).

3.6.2 Shrinkage coefficient determined from the non-linear extension

From the classical laminate theory, the curvature in principal direction of cross-ply laminate can be expressed as a function of the second derivative of the out-of-plane deformation, i.e. $K_x = \frac{\partial^2 w}{\partial x^2} = a_0$ and from eqn (3.24), $\varepsilon^0_{xx\,y=0} = a_j$. Substituting the experimental results of K_x and $\varepsilon^0_{xx\,y=0}$ into eqn (3.30) will lead to solving a system of non-linear equations to deduce the on-axis equivalent shrinkage coefficients $\gamma_{x[eq]}$ and $\gamma_{y[eq]}$.

3.7 Fisherman's net

In the previous chapter, we discussed the deformation of fabric to conform the desired component geometry during moulding. The trellis effect plays an important role in the fibre's reorientation. It was also outlined several methods used to predict the fibre's reorientation. Among them, the fisherman's model [19,20] has many advantages, and hence was chosen for fibre reorientation numerical modelling. In this model, the fabric is considered as being constituted by two families of inextensible fibres - the wefts and the warps, which connect together by the ball joints. The angle θ between a weft and a warp is a variable depicting the deformation of fabric to follow the die geometry, figure 3.3. The numerical description of this model is realised by discretizing the weft and the warp into line segments. There are three mathematical constraints were assumed.

- The first assumption is that the reinforcement fibre can neither be lengthened nor shortened during forming. The fibre ends are unconstrained and thus any axial load produced in the fibre is assumed to be negligible. The result of this assumption is that each fibre is then modelled as a series of constant length line segments joined by nodes. The mathematical constraint derived from this is that the distance between nodes on a single fibre is held fixed and we define that distance as the data point spacing, dps.

- The second assumption is based on the transverse spreading behaviour of the ply.

Transverse spreading is produced by the forming pressure. The induced squeeze flow of resin results in local thinning or thickening of the ply. As to be assumed, although ply thickness changes occur during forming, the local volume fraction does not change, and thus the transverse fibre spacing does not change. The mathematical constraint derived from this

assumption is that the distance between adjacent fibres is also held fixed and we define that distance as the fibre spacing, fs.

- The final constraint on the nodes is that they must lie on the tool surface.

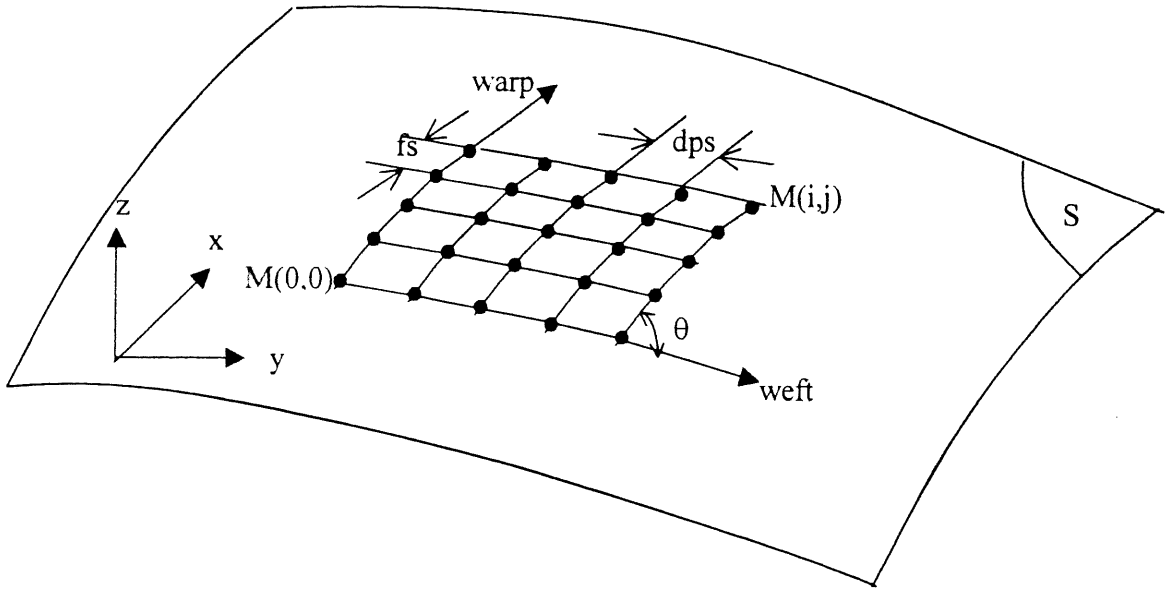

Figure 3.3 Mathematical modelling of fisherman's net.

Three above constraints can be expressed mathematically by the following equations.

$$d(M(i,j),M(i-1,j))=fs^2$$
$$d(M(i,j),M(i-1,j))=dps^2 \qquad (3.31)$$
$$M(i,j) \in S$$

Where S is surface of piece

In the cartesian coordinate system, eqn (3.31) becomes

$$(X(i,j)-X(i-1,j))^2+(Y(i,j)-Y(i-1,j)^2+(Z(i,j)-Z(i-1,j))^2=fs^2$$

$$(X(i,j)-X(i,j-1))^2+(Y(i,j)-Y(i,j-1)^2+(Z(i,j)-Z(i,j-1))^2=dps^2 \quad (3.32)$$

$$F(X(i,j),Y(i,j),Z(i,j))=0$$

Where

X(i,j), Y(i,j), Z(i,j): coordinate of point M(i,j)

F(X,Y,Z) : mathematical equation of surface tool

The iterative methods such as Newton-Raphson or Least-Squares can be used to solve these equations. The main steps are summarized as the following.

- Choose starting point $M(0,0)$. It means that the intersection between the weft and the warp, which is referred to as the reference point.
- On the weft direction, calculate points $M(i,0)$ so that $d(M(i,0),M(i-1),0)=fs$
- Repeat the second step for points on the warp direction.
- Calculate the points $M(i,j)$ by using the iterative technique and the relations in the system of equations (3.32).

3.7.1 The influence of the grid size

The fisherman's net algorithm idealizes the curve between two adjacent points on the tool surface as a line segment. Figure 3.4 represents the modelling of the tool surface curvature For a given surface, the curvature is a fixed value. Thus, the error occurring during the modelling process depends on the value of p. The more the grid size is reduced, the more the

error is reduced. However, the value of p should be chosen appropriately to avoid a lengthy calculation.

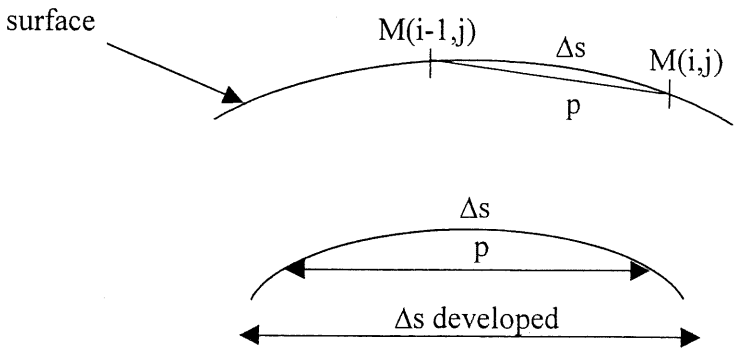

Figure 3.4 Modelling the curvature of surface.

3.7.2 Fisherman's net generalized

The fisherman's net method requires that the equation of the tool surface must be expressed in the explicit form. However, in many industrial applications, the products often have complex forms to satisfy the aerodynamic and artistic criteria. Consequently, the die geometry can not be depicted by a unique mathematical equation. To address this problem, the tool surface can be divided into small triangles (figure 3.5). The determination of the coordinates of the surface turns into that of triangles.

In the system of equations (3.31), the equation of the surface can be replaced by that of triangle in which the point M(i,j) belongs to.

$$(X(i,j)-X(i-1,j))^2+(Y(i,j)-Y(i-1,j)^2+(Z(i,j)-Z(i-1,j))^2=fs^2$$

$$(X(i,j)-X(i,j-1))^2+(Y(i,j)-Y(i,j-1)^2+(Z(i,j)-Z(i,j-1))^2=dps^2 \qquad (3.33)$$

$$A\,X(i,j)+B\,Y(i,j)+C\,Z(i,j)+D=0$$

Where

$A = (y_2-y_1)(z_3-z_1)-(y_3-y_1)(z_2-z_1)$

$B = (z_2-z_1)(x_3-x_1)-(z_3-z_1)(x_2-x_1)$

$C = (x_2-x_1)(y_3-y_1)-(x_3-x_1)(y_2-y_1)$

$D = A\,x_1 + B\,y_1 + C\,z_1$

x_i, y_i, z_i: coordinate of three nodes that constitute the triangle.

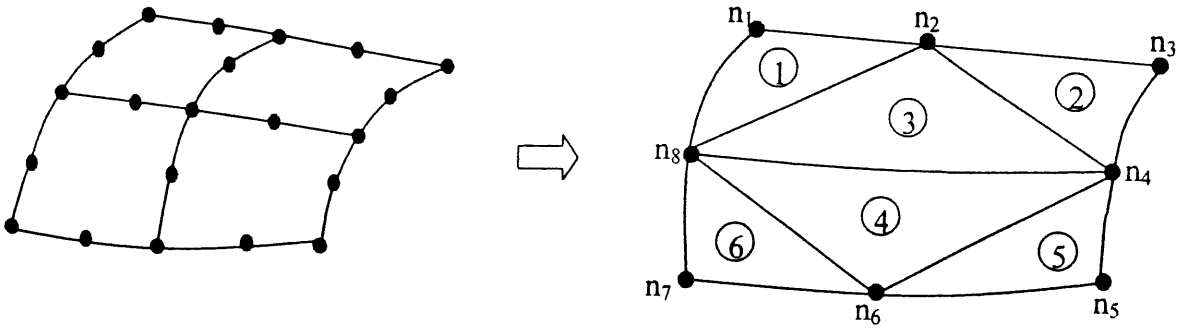

Figure 3.5 Discretisation the surface by the triangles

3.8 Finite element method

To predict strain and residual stress due to the shrinkage of resin during the moulding by the finite element method, the geometrical definition and the mechanical properties of piece must be determined. It means that the following terms must be identified

- Type of element
- Number of layers in the element.
- Material angle (wrap or weft direction in element coordinate system)
- Thickness of layer
- Engineering constants

- Geometrical definition of piece
- Boundary condition
- Applied load

The COSMOS software version 1.75A programmed by the Structural Research and Analysis Corporation was used for the finite element analysis in my research. It is also known that the rounded cone was chosen for the stress and strain analyses. This double curvature form is appropriate to the utility of the shell element with membrane and bending capabilities for analysis of three-dimensional structural models in the finite element code. Thus, the SHELL4L is the type of element used. This is a 4-node multi-layer quadrilateral thin shell element with six degrees of freedom (three translations and three rotations) per node, figure 3.6.

The shell element composes of four plies with the same anti-symmetric configuration as that of sub-plies model. It means that the stacking sequence of ply's orientation in the element coordinate system is $[0,\theta,0,\theta]$ and the corresponding thickness distribution is $[t_0/2,e/2,e/2,t_0/2]$. According to the sub-plies model, the relation between t_0 and e can be deduced from eqn (2.11).

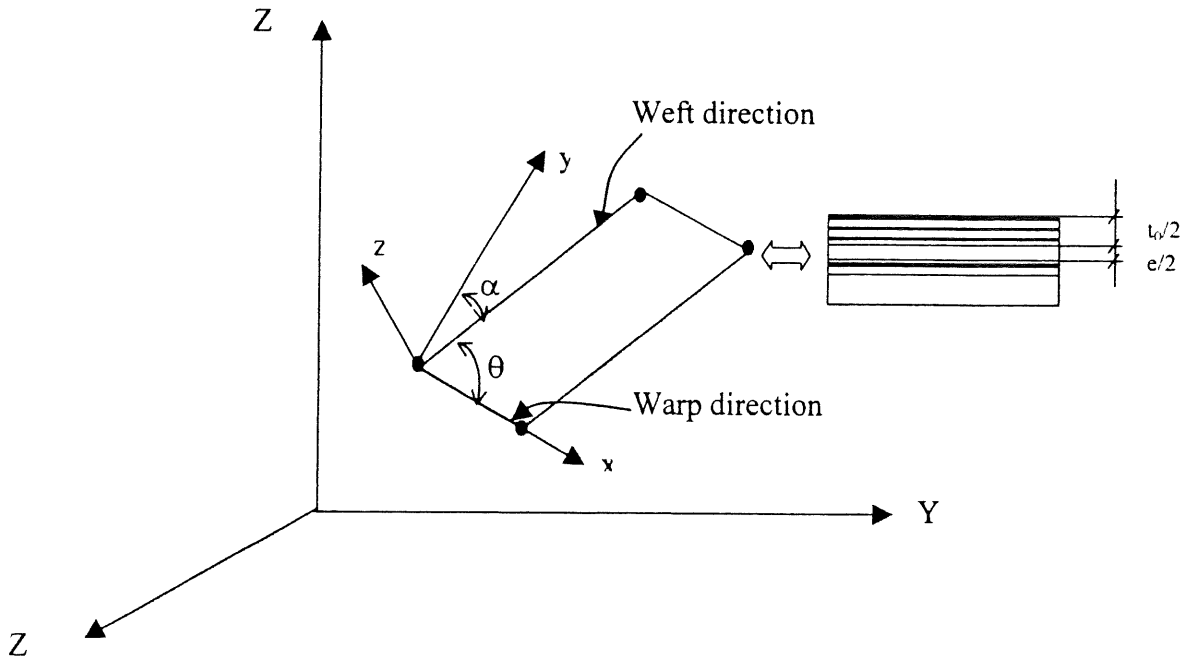

Figure 3.6 Shell4L element. XYZ: Global cartesian coordinate system. xyz: Element coordinate system.

The meshing procedure resulting from the fisherman's net method will supply the node coordinates as well as the angle θ between the weft and the warp. Pointed out in the previous chapter, the angle θ affects the total thickness according to eqn (2.2) The stiffness coefficients of the equivalent unidirectional sub-plies $Q_{xx[eq]}$, $Q_{xy[eq]}$, $Q_{yy[eq]}$, and $Q_{ss[eq]}$, determined from tension test, can be substituted into eqn 2.5 to evaluate the engineering constants.

Due to the double symmetry of piece, there is only a quadrant of piece which is modelled. The model is illustrated in figure 3.5.

The boundary conditions can be stated as the following.

For the nodes situated in the plane Y=0, the boundary conditions are

- displacement on Y is null

- rotation around Y is null
- rotation around Z is null

For the nodes situated in the plane X=0, the boundary conditions are

- displacement on X is null
- rotation around Y is null
- rotation around Z is null

The on-axis shrinkage coefficients $\gamma_{xx[eq]}$ $\gamma_{yy[eq]}$ can be applied as the thermal coefficients in condition that the variation of temperature ΔT is set to 1.

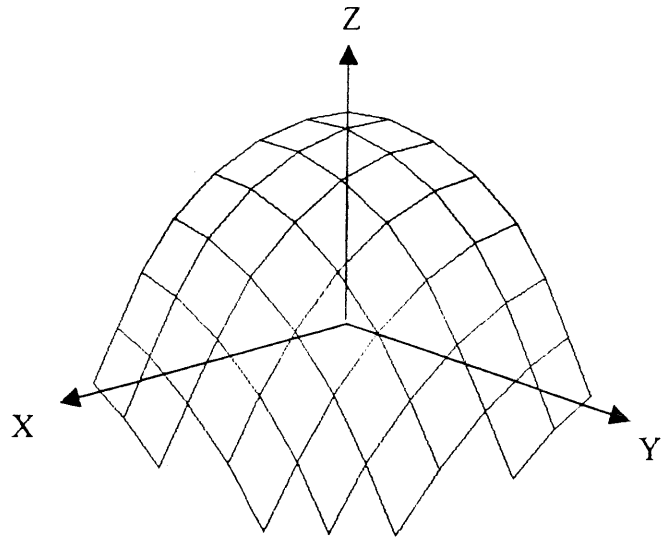

Figure 3.7 Finite element meshing for a quadrant of piece

CHAPTER IV

EXPERIMENTAL RESULTS AND DISCUSSION

4. EXPERIMENTAL RESULTS AND DISCUSSION

4.1 Materials

In order to show the effect of different fabric structures, two types of fabrics were used: a plain weave and a 8-harness satin weave. They represent two different fabric patterns commonly used (n_g=2 for plain weave and n_g=8 for 8-harness satin) with the fibre undulation effect much more important in the plain weave fabric. The thermo-elastic properties of unidirectional sub-plies without undulation were measured on a unidirectional composite consisting of the same matrix and fibres volume fraction.

All samples were fabricated by hand lay-up method from plain weave WR 180 Z, 8-harness satin (aircraft cloth 38") and AK2100 unsaturated polyester resin, supplied by Armkem Inc. Canada. An approximately 48% fibre volume fraction was maintained during the process of fabrication. The non-orthogonal fabric was made by deforming the orthogonal interlaced yarns of fabric by in-plane shearing to different angles before moulding. This in-plane deformation of the fabric was performed by clamping fabric in a fixture and shearing by hand. With this method, the angle between the weft and the warp of fabric is uniform.

4.2 Elastic properties

The mechanical properties such as the equivalent on-axis ply stiffness coefficients $Q_{xx[eq]}$, $Q_{xy[eq]}$, $Q_{yy[eq]}$, and $Q_{ss[eq]}$ were deduced from tension tests according to the ASTM (D3039). To prepare for tension test, the fabric was cut out in 0^o and 45^0 directions of fill fibres to make $[0/90]_n$ and $[-45/45]_n$ samples. The samples were cut off from the laminates by a diamond saw in order to minimize the damage. Tension test was carried out at the room

temperature and the relative humidity. Table 4.1 and 4.2 list the values of the equivalent unidirectional engineering properties and the equivalent on-axis ply stiffness coefficients that can be determined from eqn (3.2) to eqn (3.9) at the room temperature with the assumption of $E_{y[eq]} = E_{y[unidirection]}$ measured on unidirectional sample [34].

Also to be seen, the stiffness coefficients in fibre direction Q_{xx} of plain weave composite is smaller than that of 8-harness satin composite. That can be explained that due to the effect of undulation the plain weave composite becomes weaker in the fibre direction although it has the same volume fraction with the 8-harness composite.

To verify the accuracy of the above properties, the plain weave and the 8-harness satin fabric was deformed to different angles before moulding. The off-axis modulus of the deformed woven fabric composite is shown in figure 4.1 and 4.2 as a function of the angle θ between the interlaced yarns. Predictions based on sub-plies model with the equivalent unidirectional properties derived from the in-plane stiffness $Q_{xx[eq]}$, $Q_{xy[eq]}$, and $Q_{yy[eq]}$ measured on the plain weave and 8-harness satin samples and on unidirectional samples [34] are also shown. The results suggest that there is a relatively good agreement between experimental data and the prediction based on the sub-plies model. Procedures for calculating the off-axis modulus were referred from [28].

4.3 Shrinkage coefficient

4.3.1 Plain weave

To measure the shrinkage coefficient of constituent fictional ply, the plain weave fabric was deformed by in-plane shearing to an angle of 60^0. The measurement was performed on the moulded fabric samples at room temperature, after removing the specimens from the mould

for two weeks. These conditions permit the resin to complete the shrinkage process. The relative displacements ε_1 and ε_2 were measured by optical microscopy, figure 4.3. The shrinkage coefficients in the fibre direction and the transverse direction $\gamma_{x[eq]}$ and $\gamma_{y[eq]}$ were evaluated using equations (3.19) and (3.20). The shrinkage measurement is rather difficult since the shrinkage of the woven fabric composite is small with respect to the scatter of experimental measurements. The results shown in Table 4.3 are the average values determined from experimental measurements on 12 specimens. It is found that the value of $\gamma_{x[eq]}$ is positive. This implies that the resin shrinkage leads to an expansion in the fibre direction of the constituent unidirectional ply of the sub-plies model. In fact, micro-mechanical models have long been developed to predict the hydrothermal properties of a lamina. The longitudinal and transverse thermal expansion coefficients can be expressed by [35]:

$$\alpha_L = \frac{1}{E_L}(\alpha_f E_f V_f + \alpha_m E_m V_m) \tag{4.1}$$

$$\alpha_T = \alpha_f V_f + (1+\nu_m)\alpha_m V_m \tag{4.2}$$

Using the above equation, it can be seen that if shrinkage occurs only in the matrix, both the longitudinal and transverse shrinkage coefficients should be negative. The results shown in Table 4.3 are therefore quite surprising and cannot be explained by the increase in temperature during curing process.

As mentioned above, the deformations were only measured two weeks after removing the sample from the mould so that its temperature is that of room temperature. From the laminate theory, it can be shown that a positive shrinkage coefficient $\gamma_{x[eq]}$ should result in an expansion of angle-ply laminates $[+\varphi/-\varphi]_s$ for low values of φ. Figure 4.4 shows the deformation ε_1 after curing of two plain weave composites with the angles between interlaced yarns of 60° and

70°. The results confirm that curing of the matrix results in an expansion of the laminates in the direction 1, validating therefore the positive value of $\gamma_{x[eq]}$. A possible explanation for the expansion in the fibre direction of the constituent ply is that matrix shrinkage could straighten the undulated fibres in woven fabric composites. For large values of θ, it could be expected that ε_1 are negative since the coefficient $\gamma_{y[eq]}$ becomes predominant. This effect is confirmed by Figure 4.5 for the values θ of 90°, 105°, and 110°.

The values of $\gamma_{x[eq]}$ and $\gamma_{y[eq]}$ in Table 4.3 were subsequently used in the sub-plies model to predict the deformation ε_1 of the plain weave fabric, deformed to different angles θ (see Figure 4.3) . The prediction was then compared to experimental measurements. The measured data are listed in Table 4.4. Figure 4.6 presents the variation of the relative displacement ε_1 as a function of the yarns angle θ. It is seen that prediction based on the sub-plies model is in good agreement with experimental measurements. For a comparison purpose, prediction using the theoretical shrinkage coefficients calculated from Equations (4.1), (4.2) for different percentages of shrinkage of the matrix is also shown. It can be seen that the calculated shrinkage coefficients using micro-mechanics models for aligned fibres without undulation result in a very strong discrepancy between prediction and experimental measurements of shrinkage of the fabric composite after curing.

In order to verify the accuracy of this approach for predicting shrinkage due to matrix curing in woven fabric composites, measurements and calculation were carried out on orthogonal fabric samples. Eight laminates of undeformed plain weave fabric were fabricated in order to measure the relative displacement ε in the principal directions. The prediction was made by using the same shrinkage coefficients $\gamma_{x[eq]}$ and $\gamma_{y[eq]}$ in Table 4.3. The experimental results are compared to the predicted values in Table 4.5. Again, there is a good agreement between experimental measurement of shrinkage in the plain weave composite and the proposed

approach of prediction (with an error of only about 3%).

4.3.2 8-harness satin

Due to the unsymmetric woven pattern of the satin-8, the composite made of this fabric gives two types of deformation: the in-plane and out-of-plane deformations. Test data showed that the out-of-plane deformation is many times the thickness. Therefore, the non-linear extension solution was used to obtain the more precise results. The following tasks were thus carried out:

- Measure the on-axis equivalent shrinkage coefficients $\gamma_{x[eq]}$ and $\gamma_{y[eq]}$.
- Using the non-linear extension solution to improve the results.
- Study the effect of aspect ratio, mechanical properties and manufacturing parameters on shrinkage deformation.

The samples for determining the shrinkage coefficients were cut off from orthogonal 8-harness satin to the dimension of 460×90 mm^2 (aspect ratio = 5.4). This choice can help to avoid the effect of aspect ratio on test data that will be seen in the next section. Two quantities are measured: Out-of-plane deformation and in-plane strain. Non-contact measurement, using the microscope, was applied to ensure that the measurement technique did not cause any deformation on the thin laminates. It is necessary to remark that the curvature K was calculated from the out-of-plane deformation and the length of chord (see figure 4.7) by the following relationship.

$$K = \frac{8u}{c^2 + 4u^2} \tag{4.3}$$

Where:

u : out-of-plane deformation

c : length of chord

Substituting the curvature and in-plane strain into eqn (3.13) and eqn (3.14) yields the values of the on-axis equivalent shrinkage coefficients $\gamma_{x[eq]}$ and $\gamma_{y[eq]}$, see table 4.6

In order to verify the precision of these coefficients, the fabric was deformed by shear into the angles (32°, 37.5°, 45°, 52°, 55.5^{0}, 58.5^{0}) before making composite laminates. The off-axis shrinkage deformation ε_l of these laminates were measured and compared with the predicted results. The formula that deduced from equation (3.16) was used to calculate the shrinkage deformation. Figure 4.8 presents the variation of the relative off-axis displacement ε_l of angle-ply laminate as a function of deformed angle θ. It can be observed that the prediction is less accurate. The mismatch between prediction and experiment might be explained by the assumption of small out-of-plane deformation in evaluating the on-axis shrinkage coefficients. Therefore, to obtain the more precise values, the non-linear extension solution were used to determine the $\gamma_{x[eq]}$ and $\gamma_{y[eq]}$. After substituting the experimental values into eqn (3.30), the $\gamma_{x[eq]}$ and $\gamma_{y[eq]}$ can be deduced by solving simultaneously a system of non-linear equations. The results shown in table 4.6 are values determined from test data.

The contradiction in sign between $\gamma_{x[eq]}$ and $\gamma_{y[eq]}$ implies that the resin shrinkage of the constituent unidirectional ply in the sub-plies model tends to expand in the fibre direction while to shrink in the transversal direction. It is worth to note that the difference in γ_y between classical laminate theory and non-linear extension is about 15%.

Figure 4.9 shows the off-axis relative displacement in term of skew angle θ. In this case, the prediction based on the non-linear extension is in good agreement with test data.

4.4 Effect of aspect ratio on shrinkage deformation

According to the Classical Laminate Theory, the geometrical factors such as the orientation of ply angle, and the number of layers except for the geometrical dimension will affect the value of the curvatures. In contrast, for the non-linear extension, the geometrical dimension contributes to the out-of-plane deformation. In figure 4.10, the curvatures in directions: longitudinal and perpendicular to fibre, K_1 and K_2, were expressed as functions of aspect ratio. It can be seen that K_1 and K_2 become stable when the values of aspect ratio > 2. This explains why the chosen dimension for shrinkage samples is independent of the aspect ratio. It can also be seen from figure 4.10, for the aspect ratio < 2, the value of curvatures changes continuously. Thus, this area can be chosen to investigate the feasibility of non-linear extension solution. In the next section, the square plates will be used to verify the approximation of the non-linear extension solution.

4.4.1 Non-linear extension discussion

As were mentioned by some authors [14-16], the existence of in-plane shear deformation may cause the change in shape of the cured curvature, especially the shifting of bifurcation point. Thus, the effect of in-plane shear deformation was investigated. Two solutions, including and neglecting the in-plane shear strain, were carried out to clarify the influence of this factor. The initial dimensions of the laminates are 400×400 mm^2. After measuring the curvatures, successively smaller plates were cut from 400 mm square laminate such that the centre point of all the panels was the same. In the figure 4.11, the predicted principal curvatures K_1 and K_2 are plotted with different width-to-thickness ratios. The solution omits the in-plane shear strain ε_{xy}. While the predicted principal curvatures K_1 and K_2 plotted in the figure 4.12 are

calculated with the assumption of the existence of in-plane shear strain. Also in two figures, the dotted and continuous lines were drawn with the equivalent on-axis shrinkage coefficients calculated respectively from classical laminate theory and non-linear solution with and without shear analysis, table 4.6. To be observed here, the bifurcation point A [12] occurs at W/T= 125 for shear strain analysis while W/T=115 for zero-shear strain analysis. The Classical Laminate Theory and non-linear extension solutions are rather approximate at W/T=100. It is also noted that compared to the experimental results, the non-linear solution gives the better results. Moreover, for the non-linear case the shear strain analysis appears to be more converging than the zero shear strain analysis. Yet, the prediction seems to be less accurate with W/T <120 in both cases. In two analyses, the asymptotic value of curvatures reaches at W/T > 220. It can be seen from eqn 3.24, the in-plane shear strain always reaches maximum value at X=± L/2. Figure 4.13, hence, expresses the in-plane shear strain and the normal strain at middle plane in term of Y/L corresponding to X=L/2. In figure 4.14, the in-plane shear strain is expressed as a function of width to thickness ratios. Unlike the unwoven composite [14], the maximum in-plane shear strain takes place during the interval 100 < W/T < 125 and before the bifurcation point. It can also be deduced that the level of residual shear strain in cured shape is substantial in the range of 60 < W/T < 150 and negligible at both ends of the x-axis.

4.5 Effect of mechanical properties and manufacturing parameters

One of the factors that cause the deviation between theoretical calculation and experimental observation is the non-uniformity of samples due to the variations in mechanical properties, volume fraction and thickness of laminates. Especially, for the large laminates, which are fabricated by hand lay-up method, the non-homogeneity of the resin volume fraction becomes

significant. For a visualisation of the non-uniformity of sample, small specimens cut off from the square plate 400×400 mm^2 were measured for their thickness and burnt for volume fraction verification. Figures 4.15 and 4.16 give an outlook of the non-homogeneity of fibre volume fraction as well as thickness at the different plate positions. It can be seen that the values of thickness are rather scattered. To investigate the global influence of the mechanical properties on curvature value, a 10% variation of mechanical properties were supposed. Table 4.7 shows the changes in asymptotic curvature values from this change. It can be seen that the thickness and the shrinkage coefficient γ_y are the most effective on the value of curvature. That means approximately 9% variation in curvatures due to 10% of thickness and γ_y deviation. Finally, the small specimens were cut off from the composite plates and verified on the D.S.C (different scanning calorimeter) analyser for the chemical shrinkage completion. Figure 4.17 shows a typical curve of the absorbed energy of sample as a function of temperature so that the resin 's polymerisation finishes completely.

4.6 Fisherman's net verification

The Fisherman's net method is used for simulating the reorientation of fabric during moulding process. The results from this simulation are utilized for meshing procedure in finite element method. The verification of the fisherman's net model will help for selecting a suitable grid size as well as reducing the calculating error. The software called Pluton [36], based on the fisherman's net generalized method, were used for simulating the fabric reorientation during moulding process. Six rounded cones were fabricated from plain weave and 8-harness satin with the same die geometry as in figure 3.2. Figure 4.18 presents the simulation of the reorientation of fabric to follow the rounded cone shape. Due to the difficulties of measuring device, the test of fabric angle is transferred to thickness test via the relation in equation 2.2.

The following tests were realized.

- Measuring the variation of thickness in the OXY plane according to the different value of angle φ, figure 4.19. See figure 3.1 for definition of angle φ.
- Measuring the variation of thickness along with the Z axis at $\varphi = 45^0$, figure 4.20. As to be noted, the reorientation of fabric is mostly influenced at $\varphi = 45^0$.
- Verification the error occurring from grid size, figure 4.21.

In figure 4.19, t_0 is the thickness of the undeformed fabric. It means that the weft thread and the warp thread are still orthogonal. Thickness test showed that the maximum error is about 6% for two cases (plain weave and 8-harness satin).

For the error caused by crude grids, the numerical results from meshing simulation were compared to equation (3.1). The result shows that a error < 5% can be obtained with a grid size < 6mm. Therefore, a gird size =3 mm is chosen for meshing procedure in finite element method.

4.7 Finite element method application

After finishing the meshing step and choosing a suitable grid size, the calculation based on finite element method can be proceed. As to be presented in the paragraph 4.3.2, the woven composite fabricated from 8-harness satin and polyester resin give the large out-of-plane deformation. Thus, the 8-harness satin is preferred to study the deformation of piece after removing from mould. Figure 4.22 presents the top view, front view and side view of a deformed rounded cone simulated by finite element method. The deformed shape given by finite element method is the same as that of experiment, figure 4.23.

For numerical verification, two points A and B, figure 4.24, at the bottom of rounded cone

were chosen for calculating their displacements. Three different values of shrinkage coefficients calculated from the classical laminate theory, the non-linear extension with zero in-plane shear analysis, and the non-linear with in-plane shear analysis were input. Table 4.8 shows the corresponding results. According to table 4.9, the prediction with shrinkage coefficient calculated from the non-linear extension with in-plane shear analysis give the best result. Therefore, it can be concluded that the non-linear effect plays an important role on the shrinkage of polyester resin reinforced by the unsymmetric woven fabric.

TABLE 4.1 PROPERTIES OF EQUIVALENT UNIDIRECTIONAL COMPOSITE FROM PLAIN WEAVE COMPOSITE

E_x	=	36.695	(GPa)
E_y	=	7.196	(GPa)
E_s	=	5.1049	(GPa)
ν_{xy}	=	0.39	
Q_{xx}	=	37.826	(GPa)
Q_{yy}	=	7.418	(GPa)
Q_{xy}	=	2.896	(GPa)
Q_{ss}	=	5.105	(GPa)

TABLE 4.2 PROPERTIES OF EQUIVALENT UNIDIRECTIONAL COMPOSITE FROM 8-HARNESS SATIN COMPOSITE

E_x	=	38.433	(GPa)
E_y	=	7.196	(GPa)
E_s	=	5.518	(GPa)
ν_{xy}	=	0.412	
Q_{xx}	=	39.6946	(GPa)
Q_{yy}	=	7.4322	(GPa)
Q_{xy}	=	3.0621	(GPa)
Q_{ss}	=	5.518	(GPa)

TABLE 4.3 ON-AXIS SHRINKAGE COEFFICIENTS.

$\varepsilon_1\times10^{-4}$	$S^b\times10^{-5}$	$\varepsilon_2\times10^{-4}$	$S^b\times10^{-5}$	$\gamma_{x[eq]}\times10^{-4}$	$\gamma_{y[eq]}\times10^{-4}$
-3.7879	2.13698	12.197	8.4632	4.4296	-26.512

S^b : Standard deviation

TABLE 4.4 THE SHRINKAGE OF DEFORMED WOVEN FABRIC LAMINATES

Yarn 's angle of woven fabric $\theta(^{o})$	No of sample	Relative deformation on axis 1 (ε_1)	
		Mean	S^b
[+35/-35]	6	2.614×10^{-4}	5.056×10^{-5}
[+45/-45]	6	-2.462×10^{-4}	5.065×10^{-5}
[+52.5/-52.5]	6	-5.076×10^{-4}	7.829×10^{-5}
[+55/-55]	6	-7.652×10^{-4}	9.714×10^{-5}

S^b : Standard deviation

TABLE 4.5 ON-AXIS DEFORMATION DUE TO MATRIX SHRINKAGE IN ORTHOGONAL PLAIN WEAVE COMPOSITE

Experimental measurement		Prediction by sub-plies model
$\varepsilon_1\times10^{-4}$	$\underline{S^b}\times10^{-5}$	$\varepsilon_1\times10^{-4}$
1.507	1.94	1.47

S^b : Standard deviation

TABLE 4.6 EQUIVALENT ON-AXIS SHRINKAGE COEFFICIENTS

	$\varepsilon_1\times10^{-4}$	K_1	$\gamma_x\times10^{-4}$	$\gamma_y\times10^{-4}$	$\gamma_{nlx}\times10^{-4}$	$\gamma_{nly}\times10^{-4}$	$\gamma_{nsx}\times10^{-4}$	$\gamma_{nlsy}\times10^{-4}$
			Classical laminate theory		Non-linear zero shear analysis		Non-linear shear analysis	
Mean value	4.33483	4.0444	3.6786	-24.861	2.3739	-21.534	3.2047	-21.2723
Standard deviation	0.22613	0.2178						

TABLE 4.7 THE INFLUENCE OF THE VARIATION OF MECHANICAL PROPERTIES ON ASYMPTOTIC CURVATURE VALUE

	Variation of 10% value of the following mechanical properties						
	E_1	E_2	E_s	ν_{xy}	γ_x	γ_y	h
% change in K_1	3.70	-3.46	0.82	1.82	-1.03	-9.37	9.09
%change in K_2	-1.09	0.65	-0.46	-2.94	1.02	8.56	9.09

TABLE 4.8 DISPLACEMENT PREDICTED FROM FINITE ELEMENT METHOD

	experiment		Linear		Non-linear			
					zero in-plane shear analysis		in-plane shear analysis	
	ΔX(mm)	ΔY(mm)	ΔX(mm)	ΔY(mm)	ΔX(mm)	ΔY(mm)	ΔX(mm)	ΔY(mm)
Point A	8.22	0	11.412	0	7.48	0	7.67	0
Point B	0	-8.28	0	-11.47	0	-7.62	0	-7.8

TABLE 4.9 CALCULATING ERROR

	Linear	Non-linear	
		zero in-plane shear analysis	in-plane shear analysis
	error %	error %	error %
Point A	27.97	9	6.7
Point B	27.8	7.97	5.8

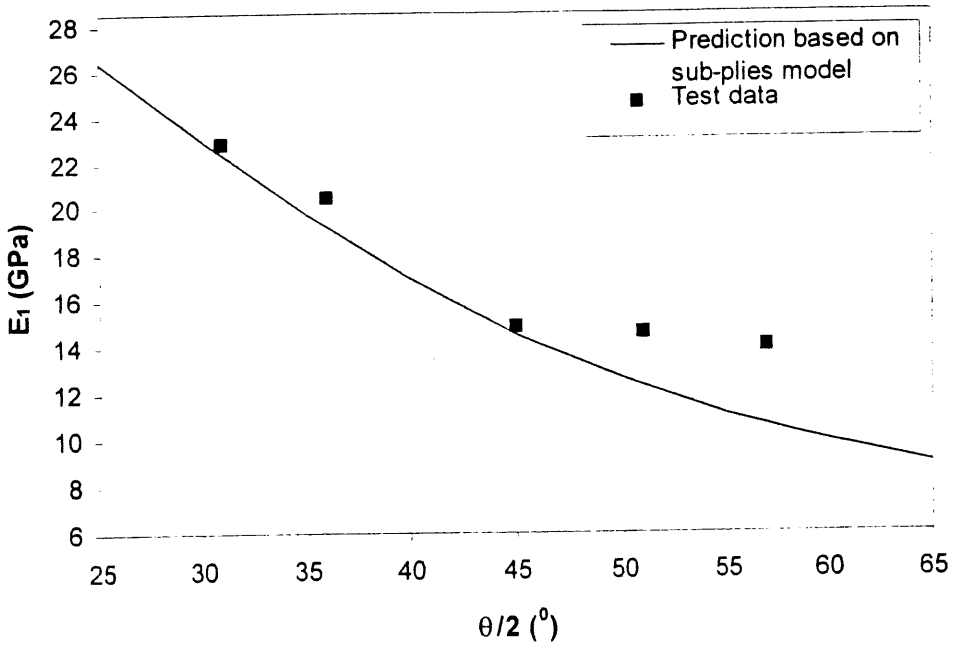

Figure 4.1 Variation of Young's modulus as a function of θ/2 for the plain weave composite

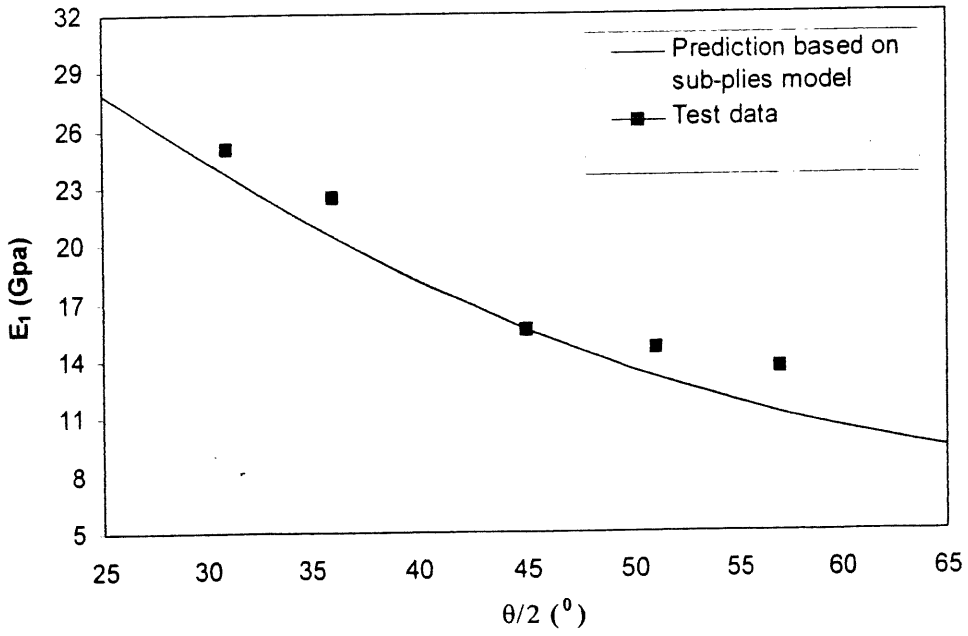

Figure 4.2 Variation of Young's modulus as a function of θ/2 for the 8-harness satin composite

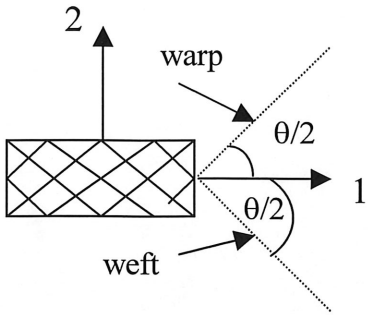

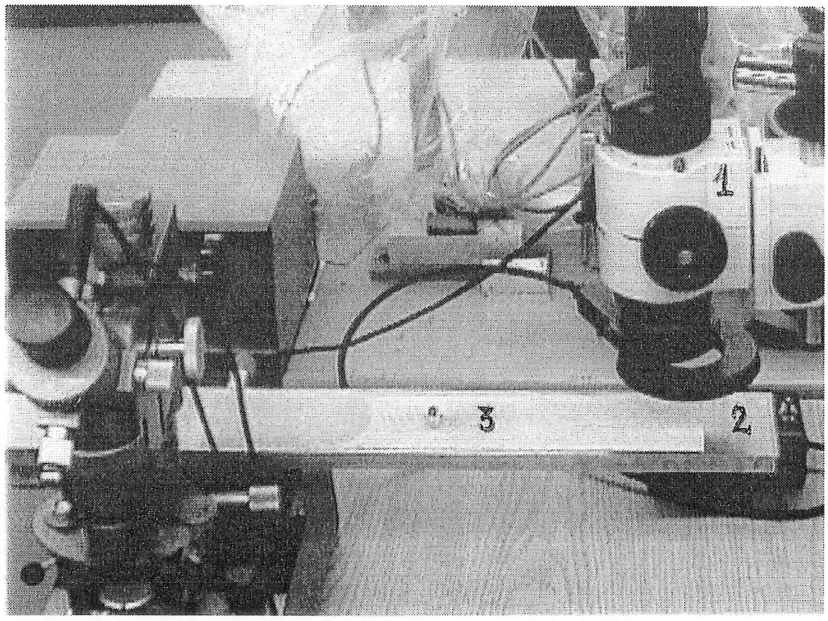

Figure 4.3 : Sample for measuring the relative displacement ε_1 and ε_2.

1) microscope, 2) tool plate, 3) sample

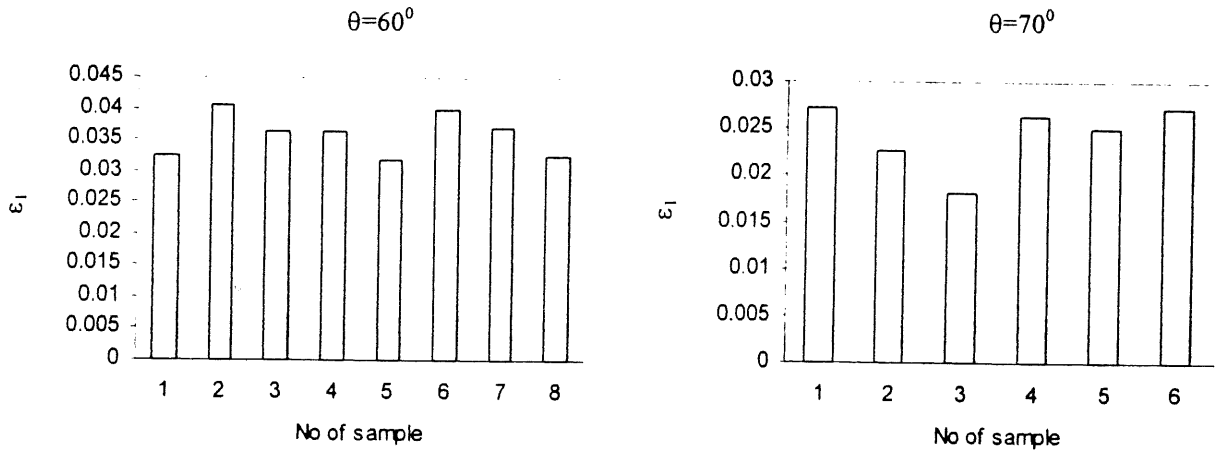

Figure 4.4 Deformation ε_l with the angles between interlaced yarns of 60°, 70°.

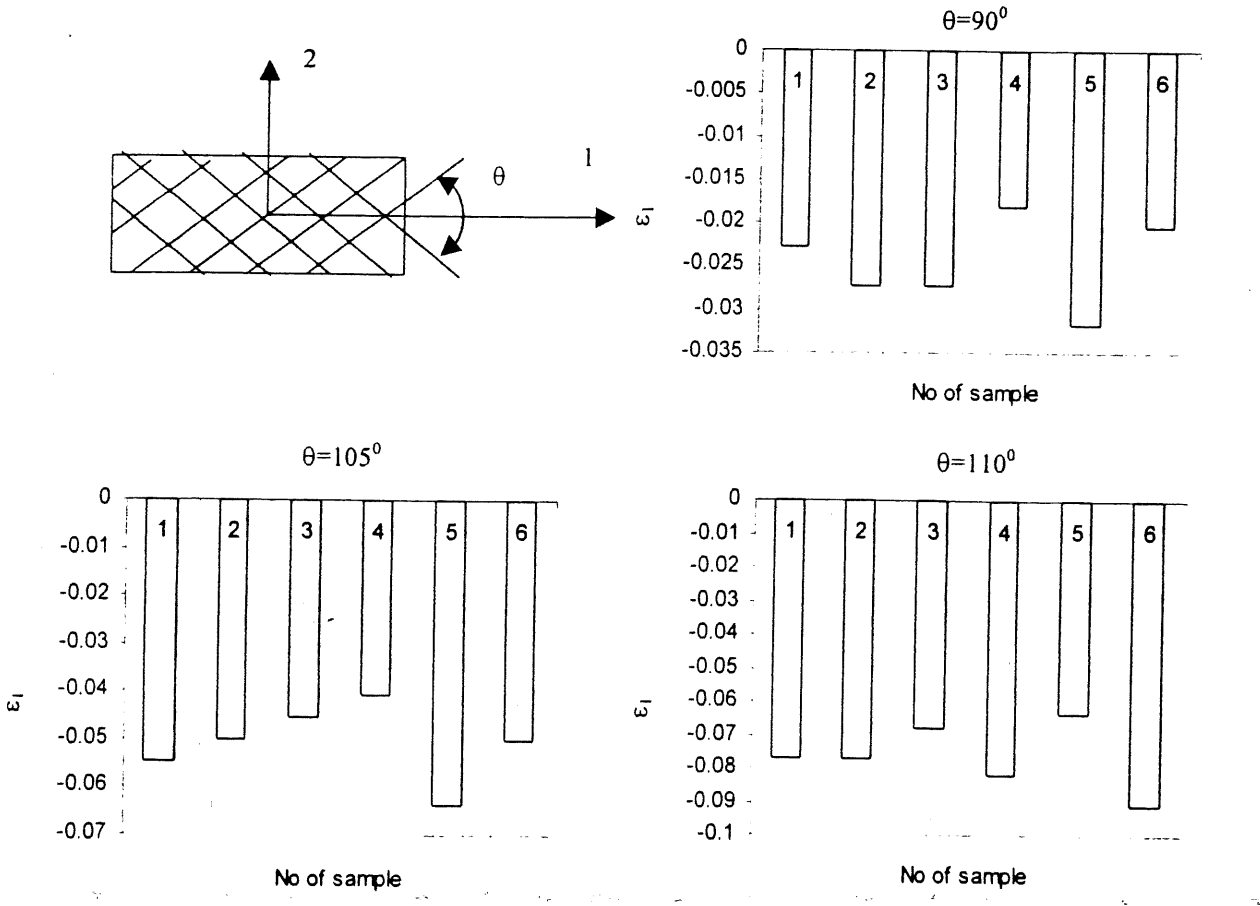

Figure 4.5 Deformation ε_l with the angles between interlaced yarns of 90°, 105°, and 110°.

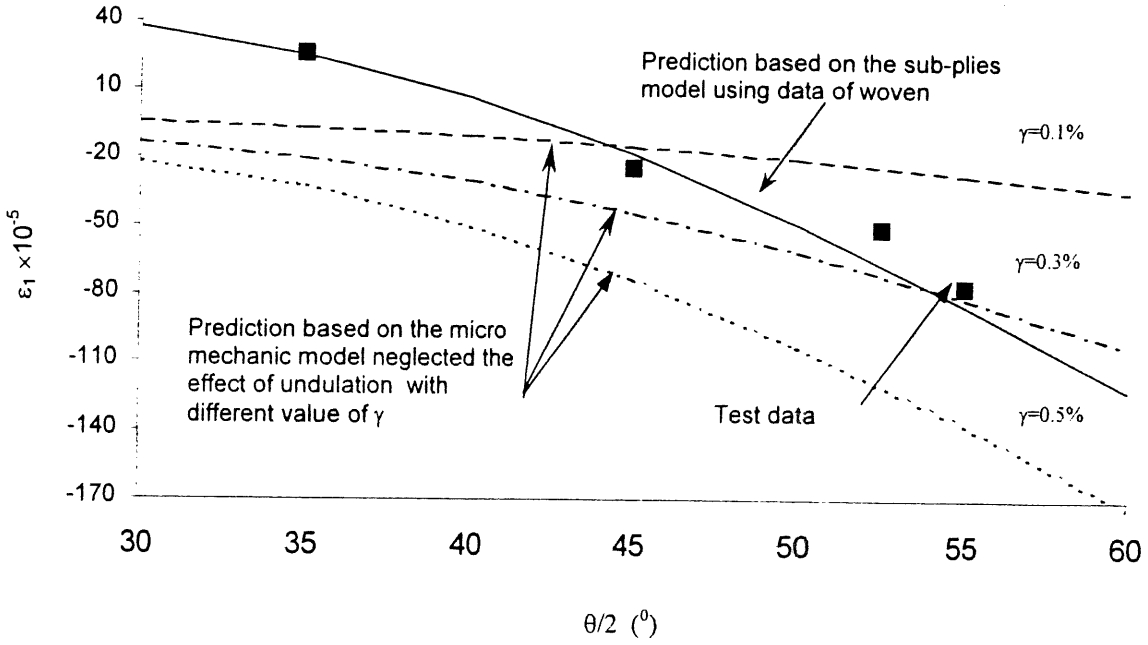

Figure 4.6 Variation of deformation due to shrinkage,ε_1 , as a function of angle θ/2. (■) : Test data; (—) : Prediction based on sub-plies model using equivalent unidirectional properties derived from experimental measurement with sub-plies model; (···),(–·),(--) : Predictions based on the micro mechanic model neglecting the effect of undulation correspond to different values of γ.

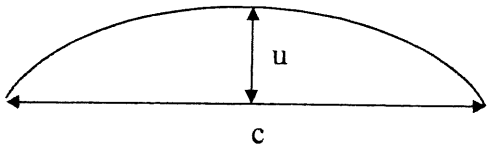

Figure 4.7 Measurement of curvature

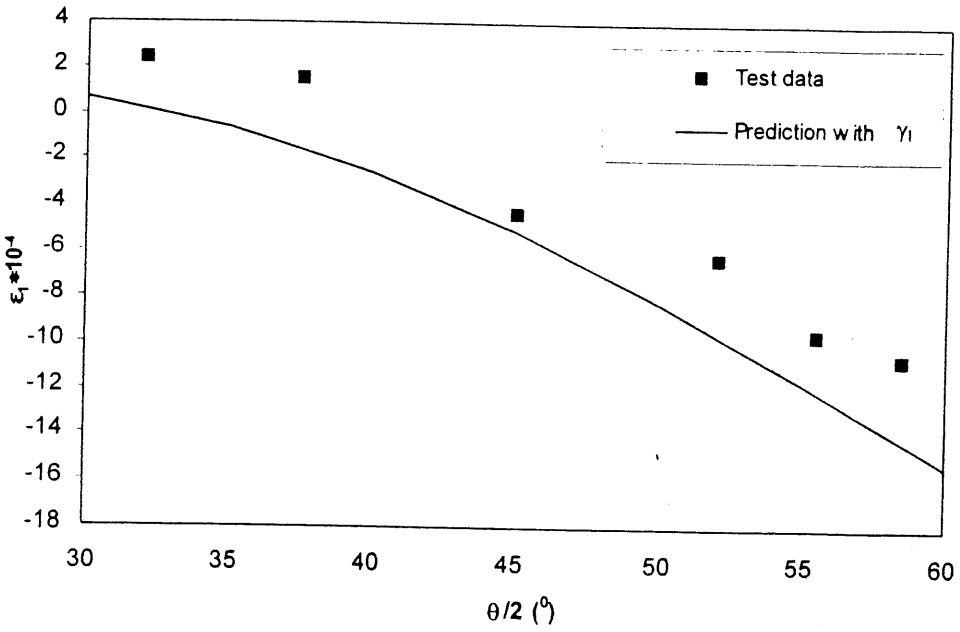

Figure 4.8 Variation of the off-axis relative displacement as a function of angle θ for 8-harness satin composite (shrinkage coefficient determined from the classical laminate theory)

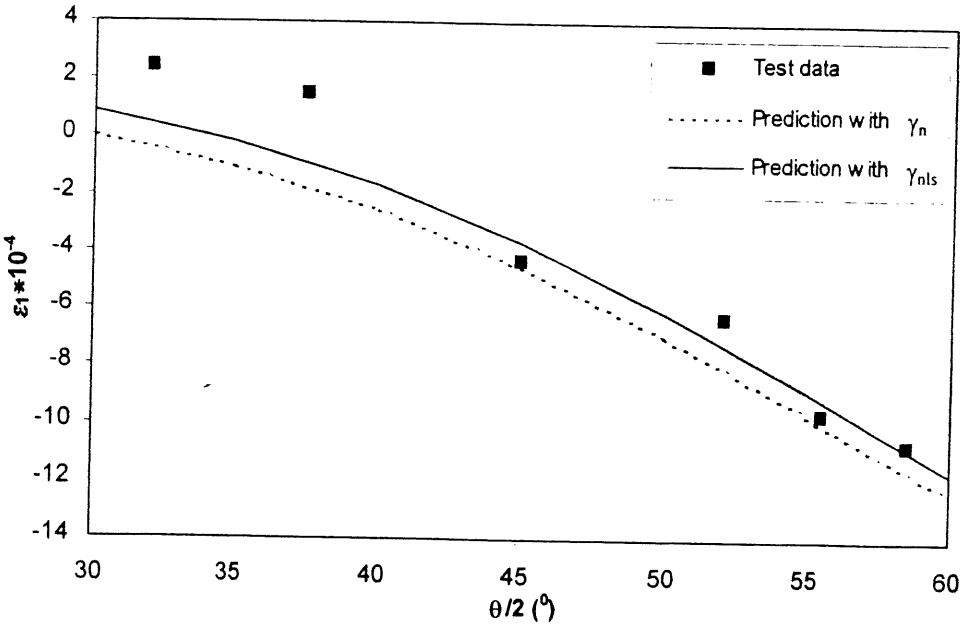

Figure 4.9 Variation of the off-axis relative displacement as a function of angle θ for 8-harness satin composite (shrinkage coefficient determined from the non-linear extension)

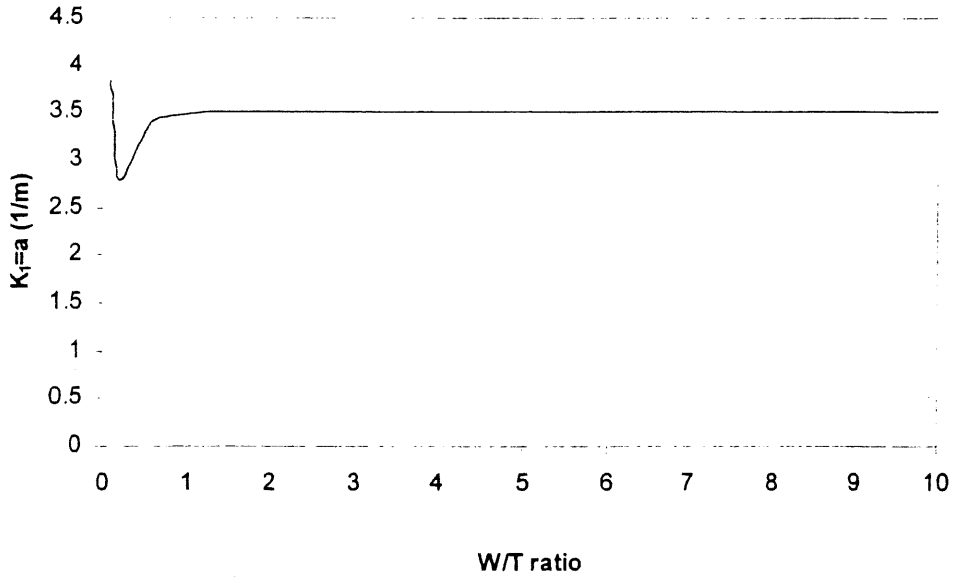

a)

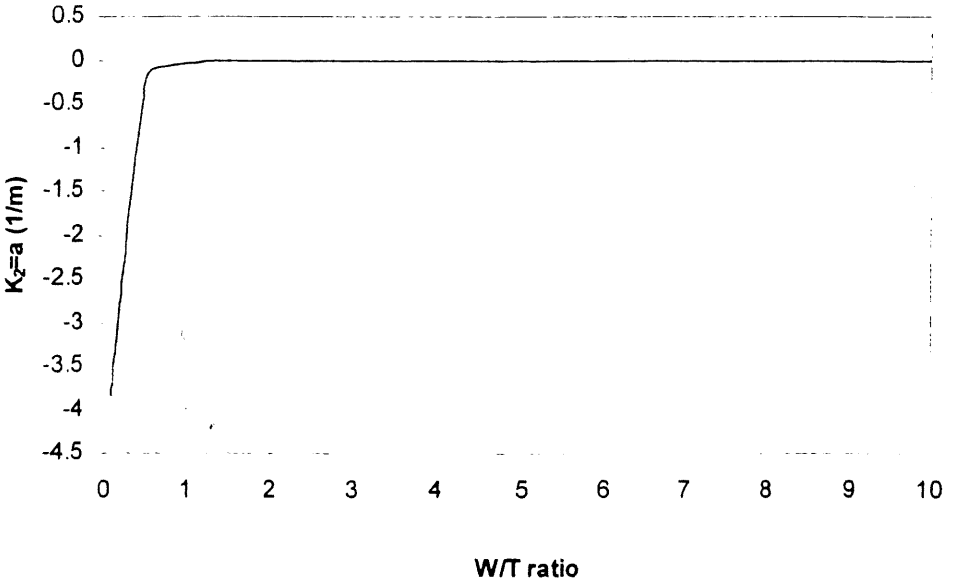

b)

Figure 4.10 Variation of curvature as function of aspect ratio. a) K_x, b) K_y

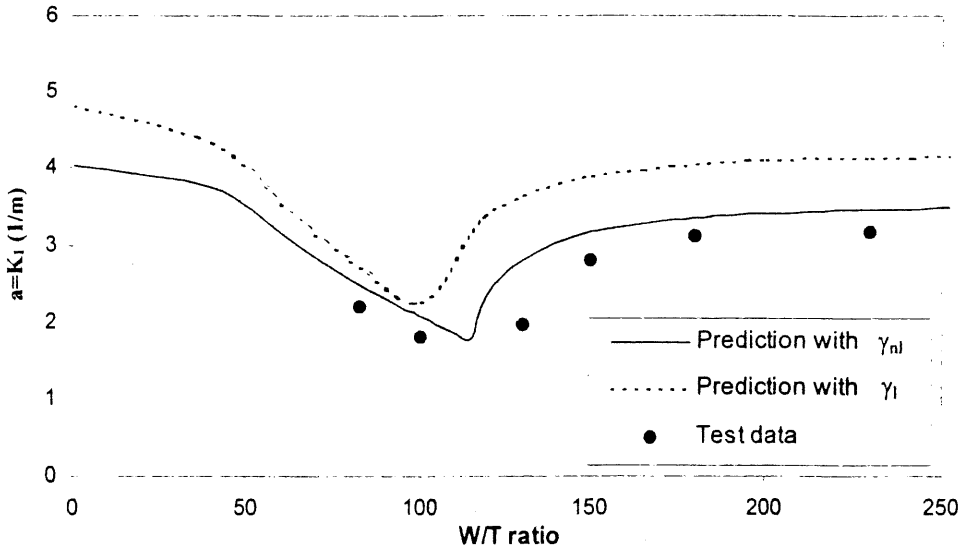

a)

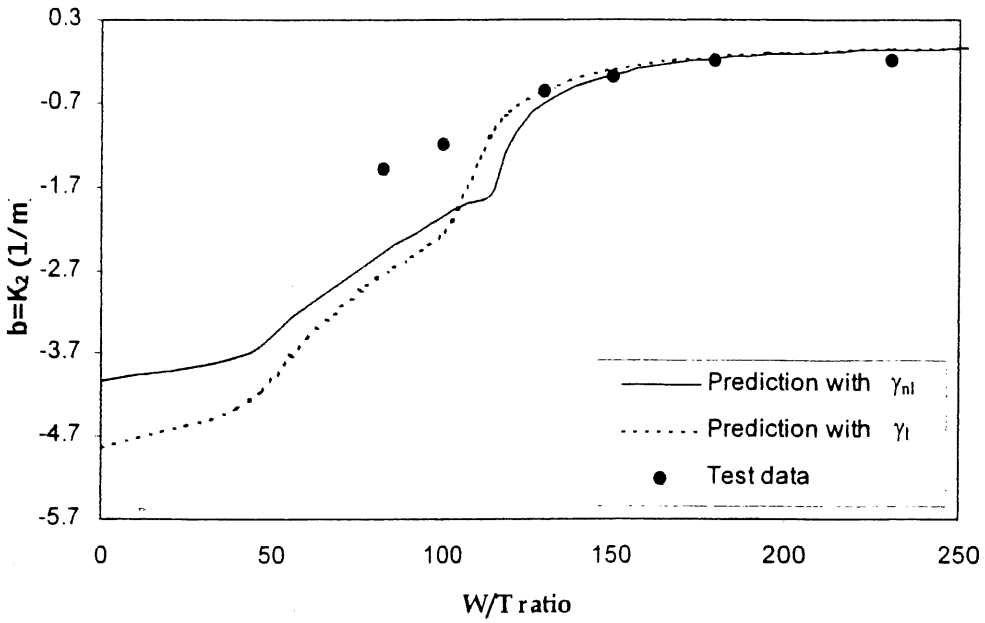

b)

Fgure 4.11 Curvature as a function of side length of 8-harness satin laminate (zero in-plane shear strain anlysis). a) K_x, b) K_y .

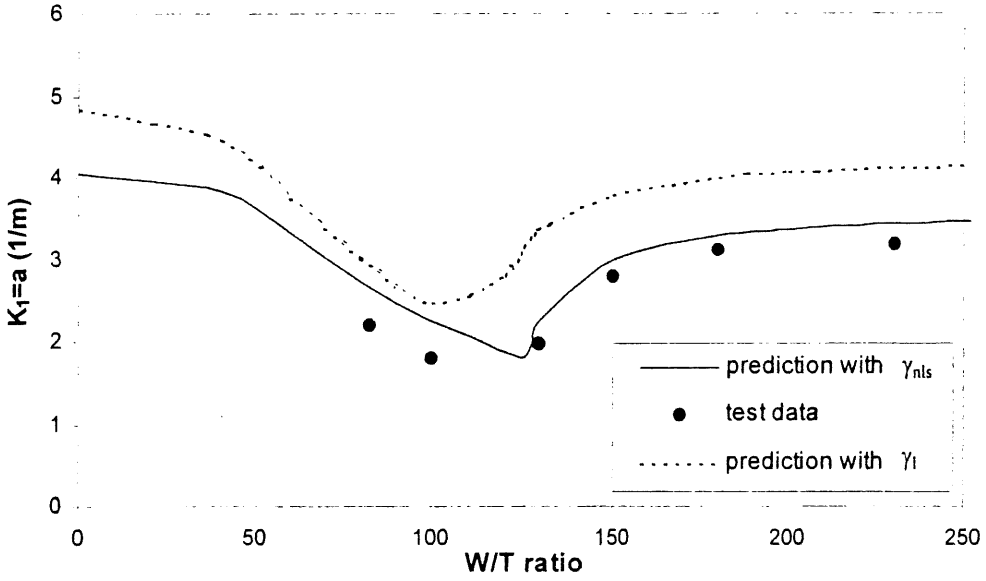

a)

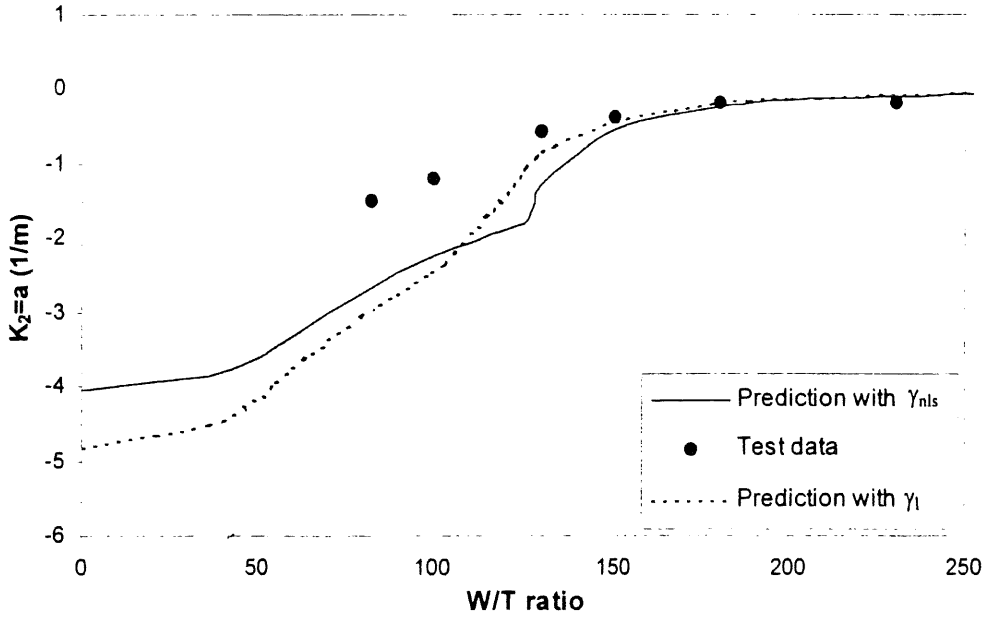

b)

Figure 4.12 Curvature as a function of side length of 8-harness satin laminate (Assumption of existence of in-plane shear strain analysis). a) K_x, b) K_y.

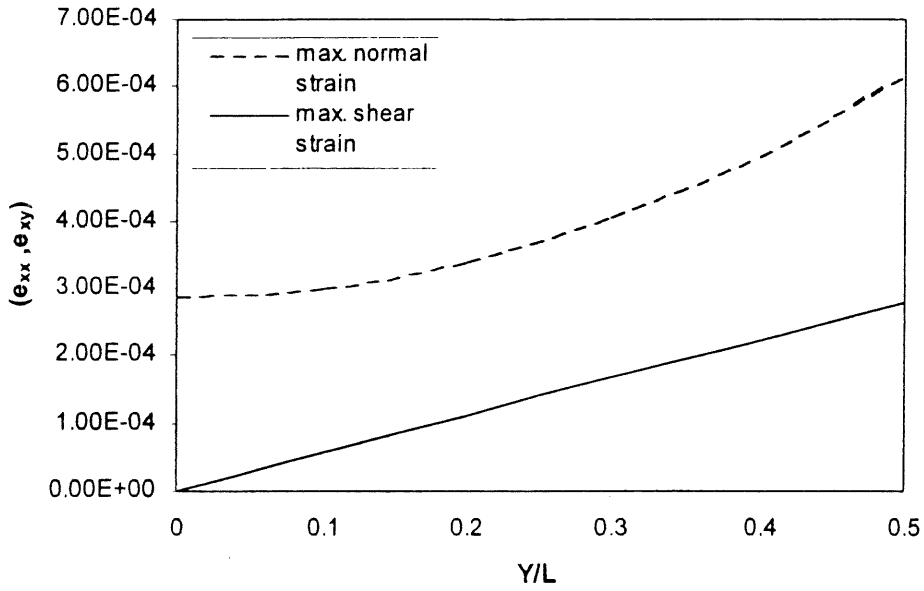

Figure 4.13 Normal strain and shear strain as functions of side length

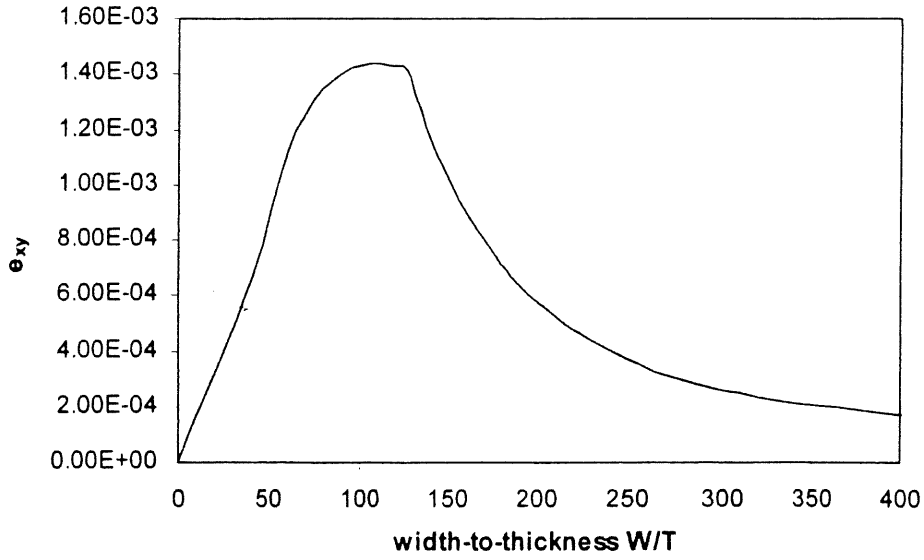

Figure 4.14 Inplane shear strain as a function of W/T

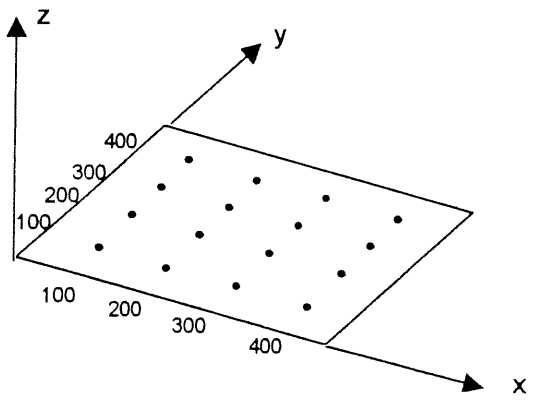

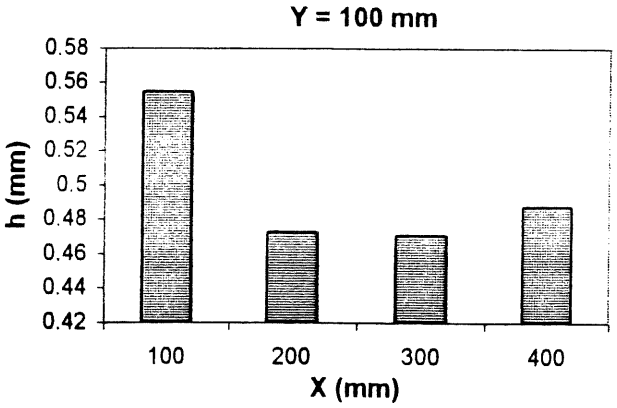

a)

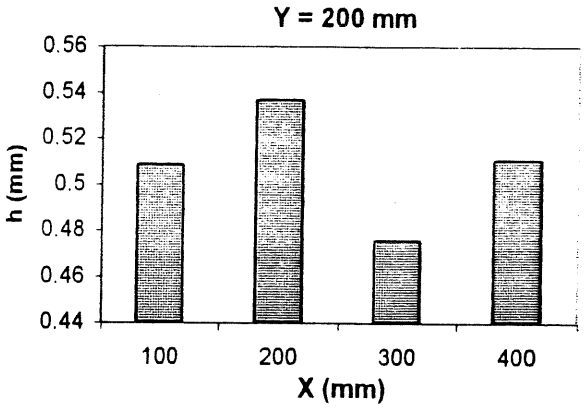

b)

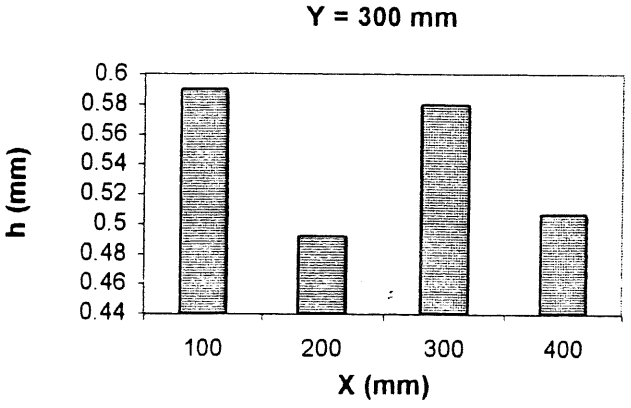

c)

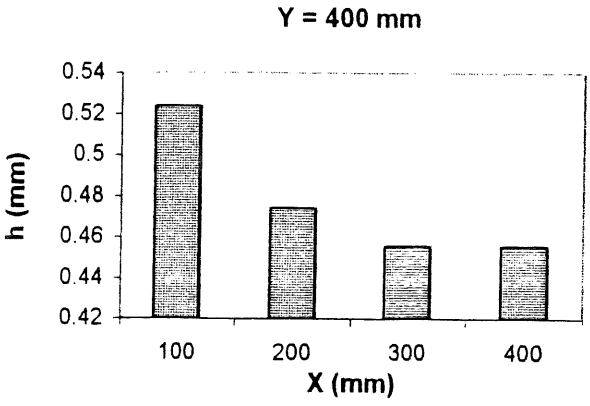

d)

Figure 4.15 Distribution of thickness on square plate 400*400 mm^2

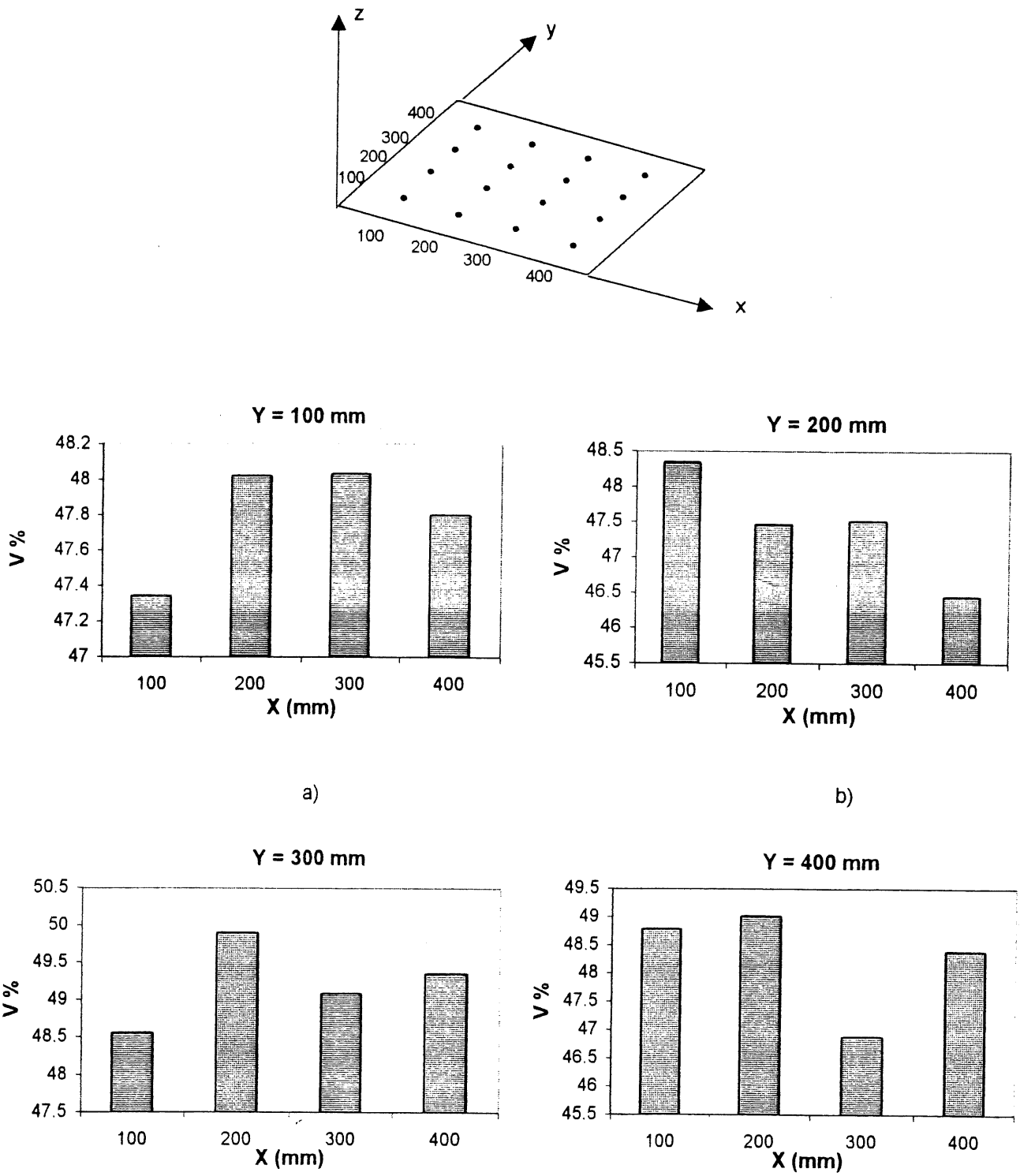

Figure 4.16 Distribution of fibre volume fraction on square plate 400*400 mm^2

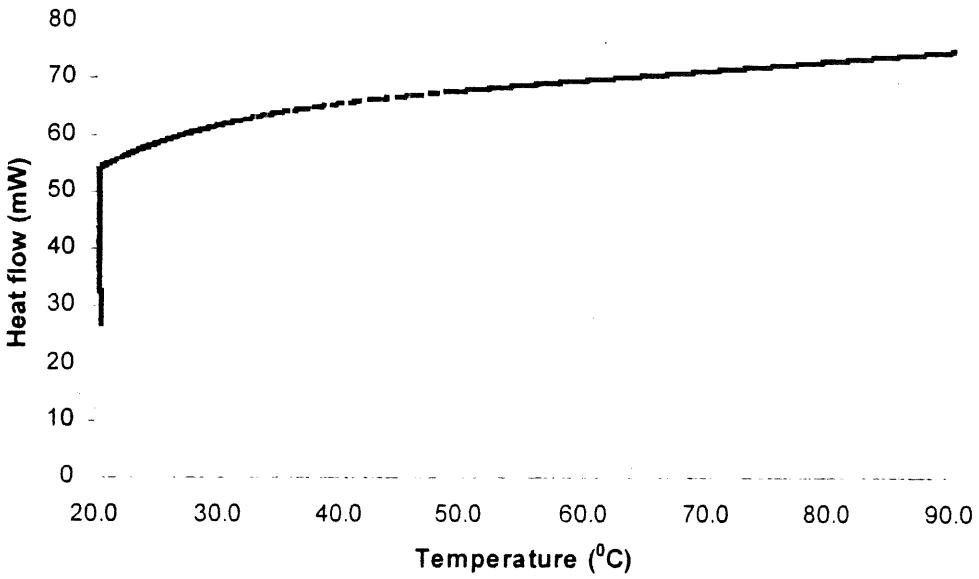

Figure 4.17 Differential scanning calorimeter for 8-haness satin composite

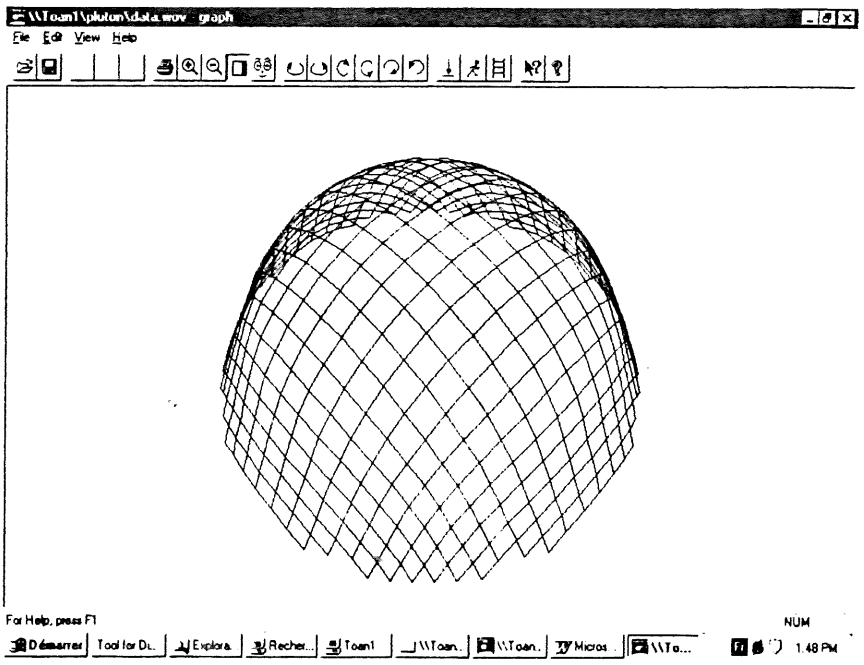

Figure 4.18 Simulation of a rounded cone by software Pluton.

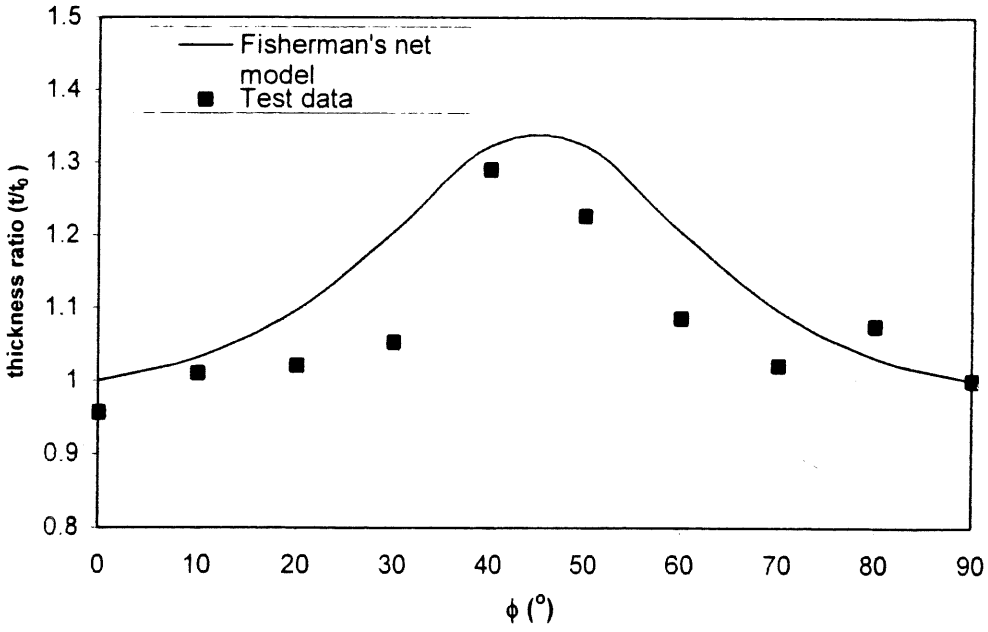

a)

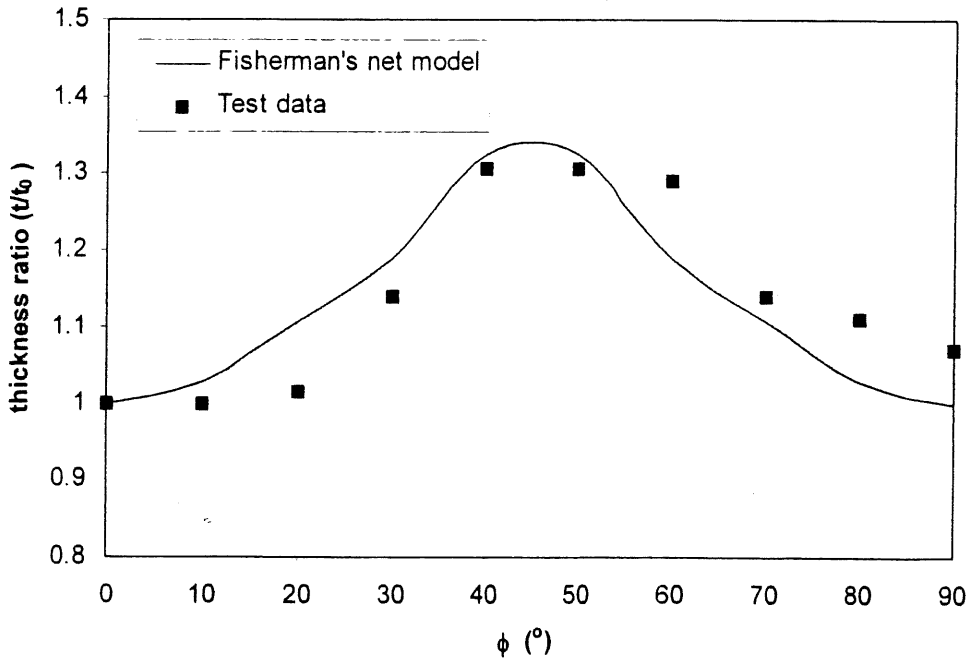

b)

Figure 4.19 Thickness ratio as a function of angle φ. a) Plain weave, b) 8-harness satin

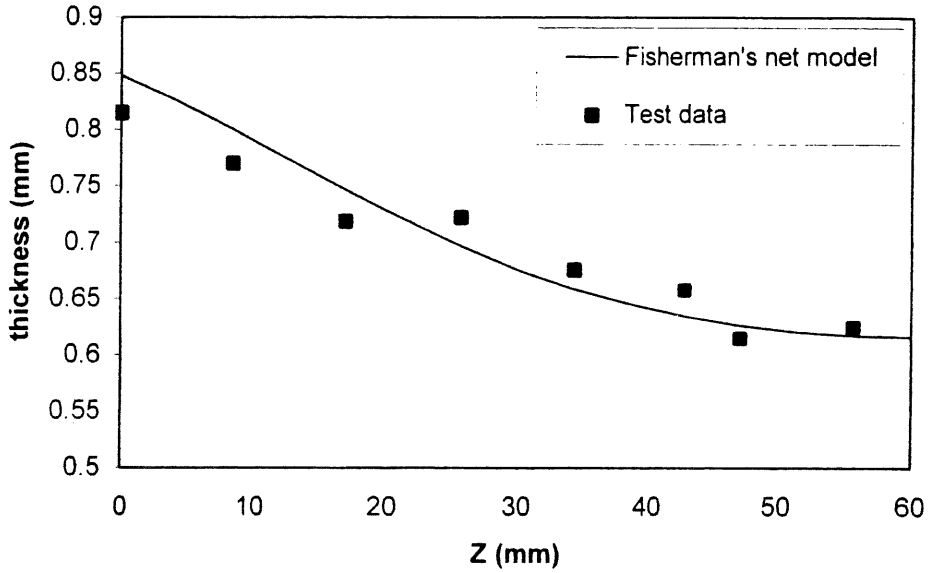

a)

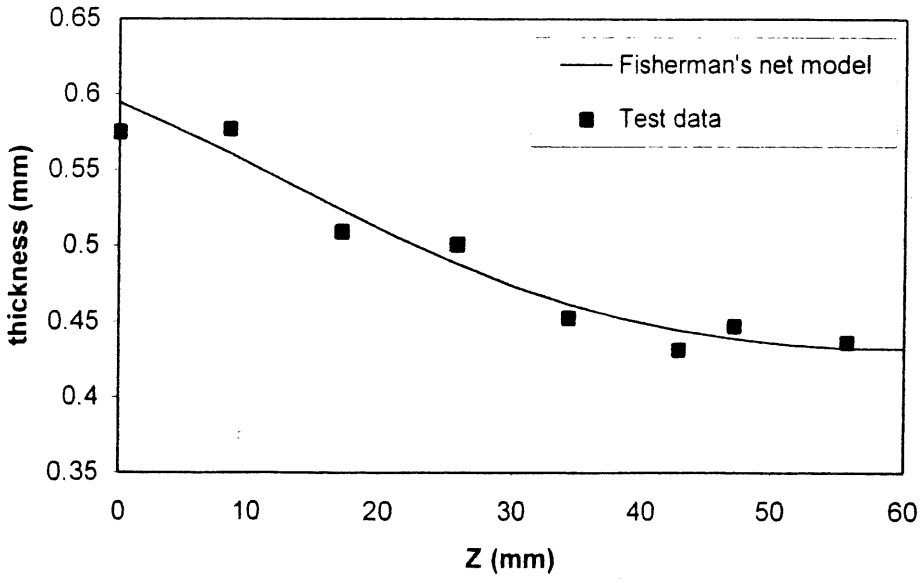

b)

Figure 4.20 Thickness versus z coordinate at $\varphi = 45^{\circ}$. a) Plain weave, b) 8-harness satin

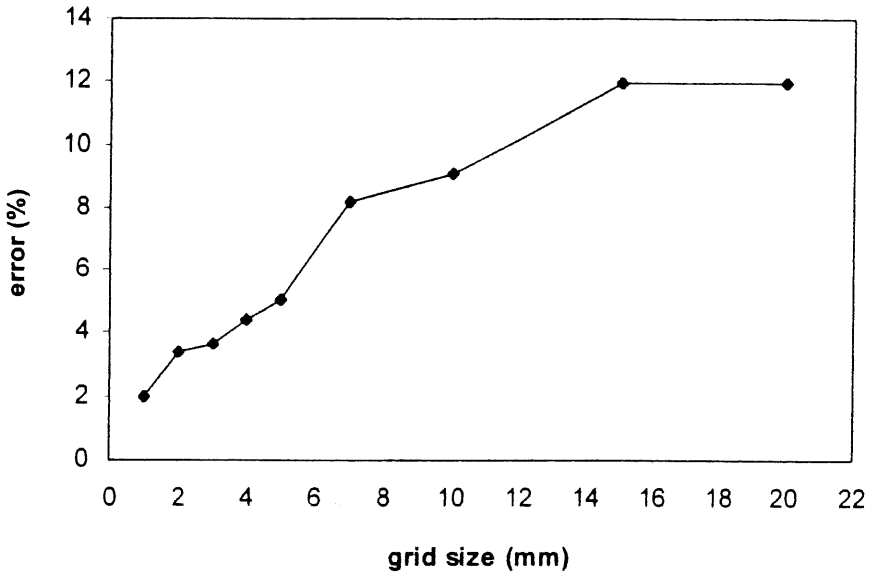

Figure 4.21 Effect of error on grid size

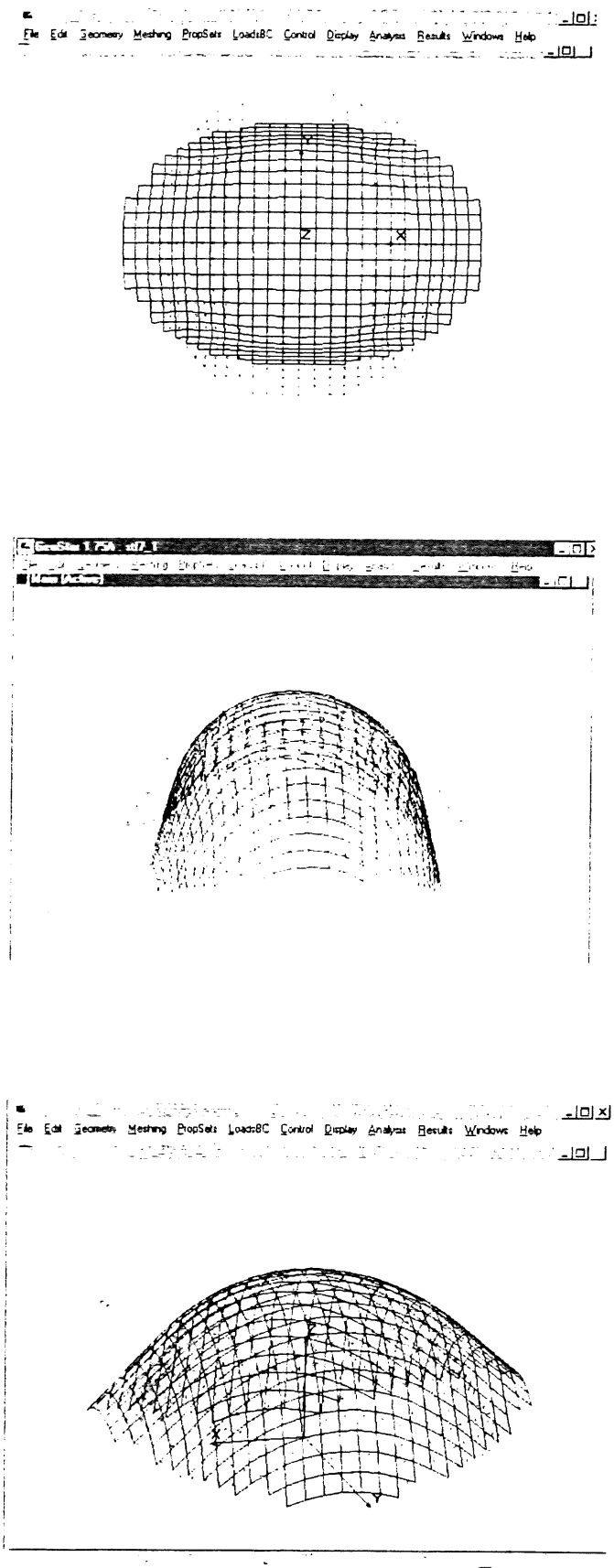

Figure 4.22 Simulation of the deformed rounded cone due to resin shrinkage by finite element method

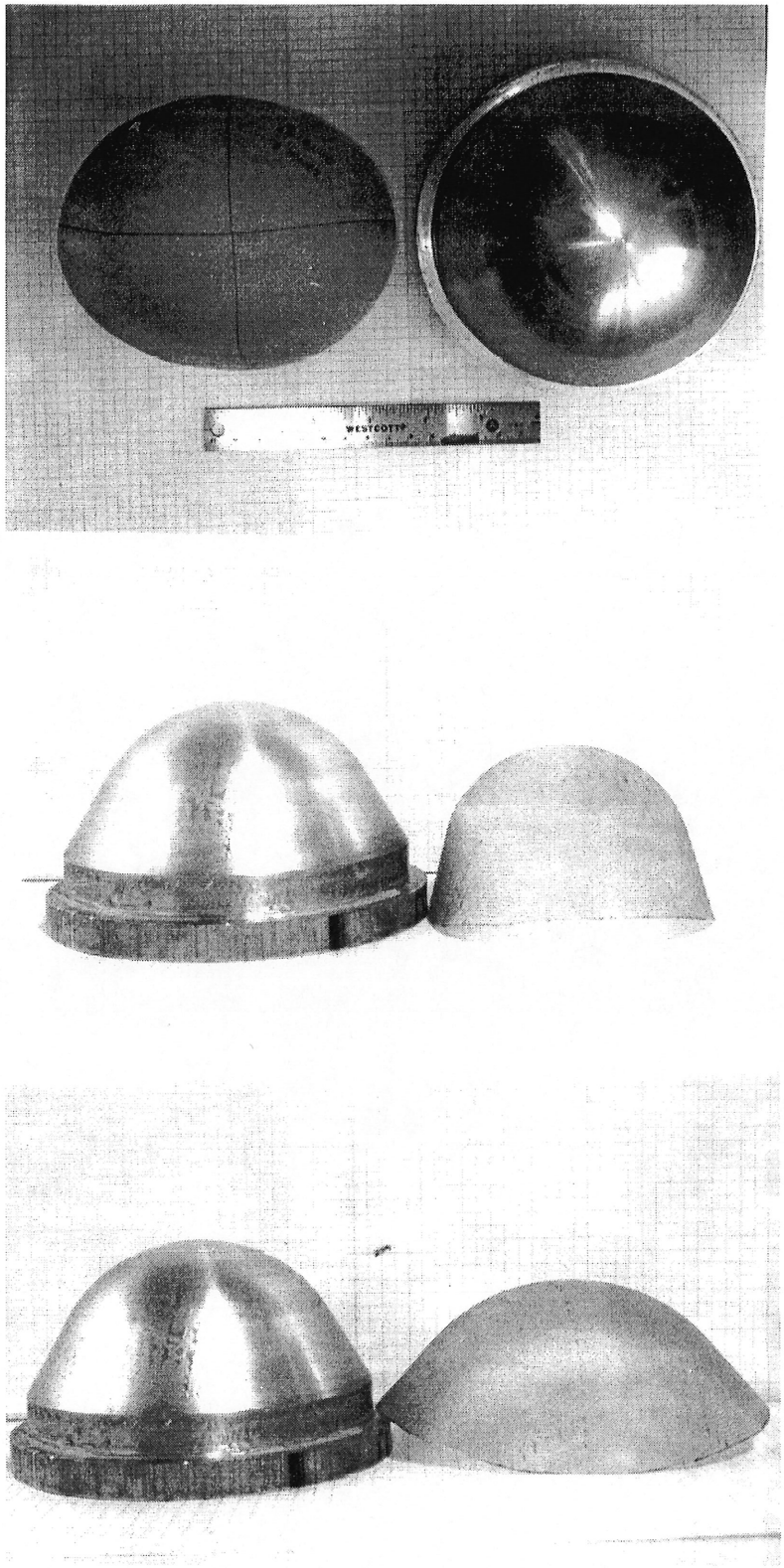

Figure 4.23 Deformation of a rounded cone

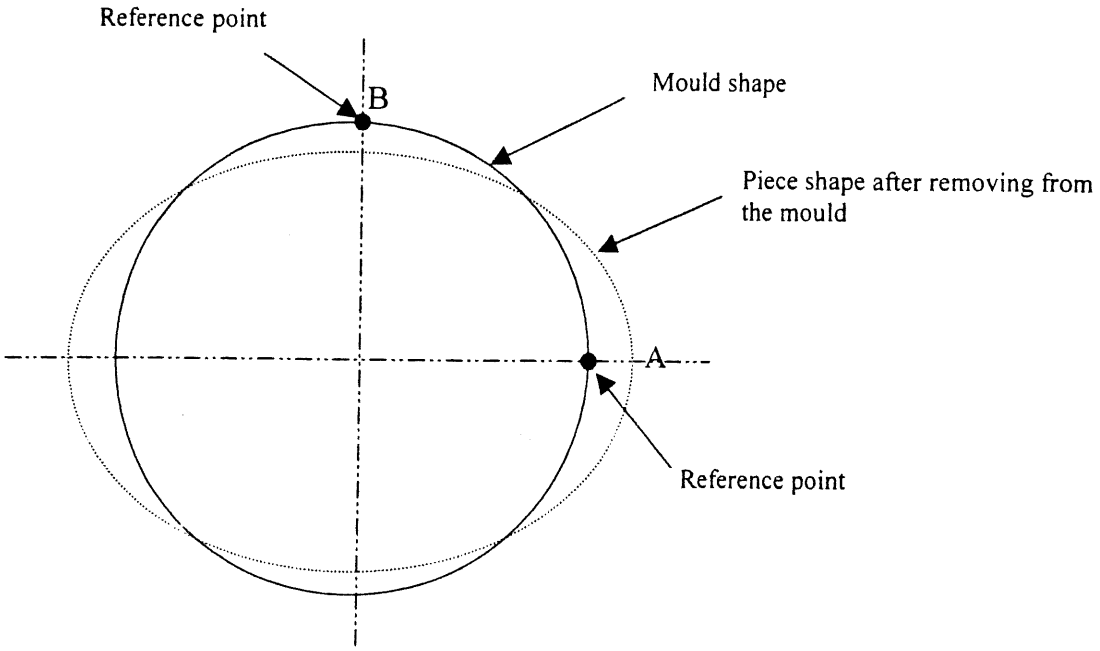

Figure 4.24 Illustration of reference points

CONCLUSION

CONCLUSION

In this work, an approach to address the shrinkage problem of polyester resin reinforced by woven fabric has been developed. The sub-plies model was used to determinate the shrinkage coefficients in woven fabric composite. Since the experimental results agree with prediction for two significant different fabric structures ($n_g = 2$ for plain weave and $n_g = 8$ for 8-harness satin), it is expected that the model will also be applicable to other common woven fabric structures ($2 < n_g < 8$) as well. To take into account the fibre undulation effect, the on-axis thermo-elastic properties of the fictional constituent plies in the sub-plies model can be determined by an experimental procedure. The research on the shrinkage problem showed some interesting results. The resin tends to shrink in the direction perpendicular to the fibre direction while to extend in the fibre direction. For the laminates fabricated from unsymmetric woven fabric such as 8-harness satin, there is a large out-of-plane deformation after removing the laminate from the mould. Thus, to obtain a precise evaluation of shrinkage coefficients, the non-linear solution was used. The prediction, based on the non-linear solution, conforms to the experiments. The study also showed that aspect ratio and width to thickness ratio affect on the value of curvature of laminate. Finally, the rounded cones were fabricated from polyester resin and 8-harness satin to verify the sub-plies model. The results from experimental measurements and those calculated are different about 5%.

REFERENCES

REFERENCE

1] M. Ruffier, G.Merle, J.P.Pascault, " The Shrinkage Compensation Of Unsaturated Polyester Resins- Polyvinyl Acetate Blends Polymerization Proceeds Through Fractal Morphologies: Characterization And Simulation ", Journal of Materials Sciences 31 : 4679-4687, 1996.

[2] Huang, Yan-Jyi, Liang, Chiou-Ming, " Volume Shrinkage Characteristics In The Cure Of Low-Shrink Unsaturated Polyester Resins ", Polymer 37: 401-412, 1996.

[3] Saito, R.; Kan, W.-M.J.; Lee, L.J, " Thickening Behaviour and Shrinkage Control of Low Profile Unsaturated Polyester Resins", Polymer 37: 3567-3576,1996.

[4] Huang, Yan-Jyi, Liang, Chiou-Ming, " Effect of Low-Profile Additives on Volume Shrinkage Characteristics in The Cure of Unsaturated Polyester Resin ", Annual Technical Conference – ANTEC, Boston, MA, USA, 1995.

[5] Piggott, M.R., Zhou, W. " Shrinkage Control In Fiber Reinforced Polymers III : Carbon Fibre Reinforced Polyesters With Expanding Monomers And Low Profile Additives", Polymer & Polymer Composites, vol.3 n 6: 395-402, 1995.

[6] Ahang, L.Ernst, L.J, Brouwer, H.R., " Transverse Behavior of a Unidirectional Composite (Glass Fibre Reinforced Unsaturated Polyester). Part II. Influence of Shrinkage Strains'', Mechanics of Materials, vol.27 n 1: 37-61, 1998.

[7] Shih, Wayne K., " Shrinkage Modeling of Polyester Shrink Film '', Polymer Engineering and Science, 43: 1121-1128, 1994.

[8] Shi-Chang Tseng and Tim A. Osswald, "Prediction of Shrinkage and Warpage of Fiber Reinforced Thermoset Composite Parts'', Journal of Reinforced Plastics And Composite 13: 698-721, 1994.

[9] S.F. Walsh, " Shrinkage and Warpage Prediction for Injection Molded Components'', Journal of Reinforced Plastics And Composite 12 : 769-777,1993.

[10] Takashi Ishikawa, "Anti_symmetric Elastic Properties of Composite Plates of Satin Weave Cloth'', Fibre Science & Technology, 15: 127-145,1981.

[11] Michael W.Hyer. " Some Observations on the Cured Shape of Thin Unsymmetric Laminates'', J. Composite Materials, 15: 175-191, 1981.

[12] Michael W.Hyer, " Calculation of the Room-Temperature Shapes of Unsymmetric Laminates'', J. Composite Materials, 15: 296-310,1981.

[13] Michael W.Hyer. " The Room-Temperature Shapes of Four-Layer Unsymmetric Cross-Ply Laminates'', J. Composite Materials, 16: 318-340,1981.

[14] Jun, W.J. and C.S. Hong, "Effect of Residual Shear Strain on the Cured Shape of Unsymmetric Cross-Ply Thin Laminates'', Comp. Science and Technology, 38: 55-67, 1990.

[15] Peeters, L.J.B.,P.C.Powell and L.Warnet, " Thermally-Induced Shape of Unsymmeric Cross-Ply Thin Laminates'', J. Composite Materials, 30: 603-626,1996.

[16] Maenghyo Cho and Min-Ho Kim, "A Study on the Room-Temperature Curvature Shapes of Unsymmetric Laminates Including Slippage Effects'', J. Composite Materials, 32: 460-482, 1998.

[17] Materials Sciences Corporation, "Woven Fabric Reinforced Composites for Automotive Applications'', Technical Final Report, National Science Foundation Grant N^0 DMR-8212867, MSC TFR 1605/8102, 1985.

[18] Van Der Weeen, F., "Algorithms for Draping Fabrics on Doubly-Curved Surfaces'', International Journal of Numerical Methods in Engineering, 31: 1415-1426, 1991.

[19] Roberstion, R.E., Hsiue. E.S., "Fibre Rearrangements During the Molding of Continous Fiber Composites. I. Flat Cloth to a Hemisphere'', Polymer Composites, 2: 126-131, 1981.

[20] Roberstion, R.E., Hsiue. E.S., "Continous Fibre Rearrangements During the Molding of

Fiber Composites. II. Flat Cloth to a Rounded Cone'', Polymer Composites, 5: 191-197, 1984.

[21] Gutowski, T.G ., Cai, Z., Soll, W., and Bonhomme, L," The Mechanic of Composites Deformation During Manufacturing Processes'', Proceedings of the American Society for Composites, 1st Technical Conference, vol.1, 1986.

[22] Cogwell, F.N. and Leach, D.C.," Processing Science of Continuous Fibre Reinforced Thermoplastic Composites'', 33 rd International SAMPE Symposium, vol. 33, 1988.

[23] Laroche, D. "Prediction des contraintes et déformations résiduelles obtenues lors du moulage de formes complexes en composite stratifié'', Mémoire de Maitrise, École Polytechnique de Montréal, 1991.

[24] Hahn, H.T. and Pagano, N.J.," Curing Stresses in Composite Materials'', Journal of Composite Materials, 9: 91-106, 1975.

[25] Hahn, H.T., " Residual Stresses in polymer Matrix Composite Laminates'', Journal of Composite Materials, 10: 266-278, 1976.

[26] Kim, K,S., Hahn, H.T. and Croman, R.B., "The Effect of Cooling Rate on Residual Stress in a Thermoplastic Composite'', Journal of Composite Technomology and Research, 11: 47-52, 1989.

[27] Kim, K.S. and Hahn. H.T., "Residual Stress Development during Processing of Graphite/Epoxy Composites'', Composites Science and Technology, v.36, 121-132, 1989.

[28] Tsai, S.W. and Hahn, H.T., "Introduction to Composite Materials'', Technomic Publishing Company, Inc. Lanscater, Pennsylvania, 1980.

[29] Ishikawa, T.," Anti-Symetric Elatis Properties of Composites Plates of Satin Weave Cloth'', Fibre Science and technology, 15: 127-145, 1981.

[30] Ishikawa, T. And Chou T.W., "Stiffness and Strength Behavior of Woven Fabric Composites'', Journal of Materials Science, 17: 3211-3220, 1982.

[31] Ishikawa, T., Matsuhima, M., Hayashi, Y. and Chou, T.W., "Experimental Confirmation

of the Theory of Elastic Moduli of Fabric Composites'', Journal of Composite Materials, 19: 443-458, 1985.

[32] Laroche, D. And Vu-Khanh, T., "Modeling of the Thermo-Elastic Properties of Woven Fabric Composites in Complex Shapes, Composite Materials: Testing and Design, 11: 263-275, 1993.

[33] T. Vu-Khanh and B. Liu, "Prediction of Fibre Rearrangement and Thermal Expansion Behaviour of Deformed Woven-Fabric Laminates``, Composites Science and Technology, 53: 183-191, 1995.

[34] H. Nguyen Hoa and T. Vu Khanh, "Prediction of Failure in Unsaturated Polyester Reinforced by Plain Weave Glass Fabric'', Design and Manufacturing of Composite. Technomic publication, 224-234, 1998.

[35] Kuno K.U. Stellbrink, "Micro mechanics of Composites'' Hanser/ Gardner Publication, Inc., Cincinnati. 1996.

[36] Yves Baillargeon, "Calcul Sur la Déformation Des Composites à Reinfort Tissé Après Formage'', Mémoire de maîtrise en sciences appliquées, Université de Sherbrooke, 1998.

APPENDIX

APPENDIX A

With zero in-plane analysis, system of equation (3.30) has the following form

$$A_{11}^s(a_1 - a_0b_0C_2) - B_{11}^s a_0 + A_{12}^s(b_1 - C_1a_0b_0) - N_x = 0$$
$$A_{12}^s(a_1 - C_2a_0b_0) + B_{22}^s b_0 + A_{22}^s(b_1 - C_1a_0b_0) - N_y = 0$$
$$A_{11}^s(C_4a_0^2b_0 - C_2a_0a_1) + A_{12}^s(2a_0^2b_0C_3 - C_2a_0b_1 - a_0a_1) - A_{22}^s(C_4a_0^2b_0 - C_1a_0b_0) +$$
$$B_{11}^s c_2a_0^2 + B_{22}^s(C_1a_0b_0 - b_1) + D_{12}^s a_0 + D_{22}^s b_0 + (C_2N_x + C_1N_y)a_0 + M_y = 0$$
$$A_{11}^s(C_5a_0b_0^2 - C_2a_1b_0) + A_{12}^s(2a_0b_0^2C_3 - C_1a_1b_0 - c_2b_1) - A_{22}^s(C_4a_0b_0^2 - C_1b_0b_1) +$$
$$B_{11}^s(2a_0b_0C_2 - a_1) + B_{22}^s C_1b_0^2 + D_{11}^s a_0 + D_{12}^s b_0 + (C_2N_x + C_1N_y)b_0 + M_y = 0$$

where

$$C_1 = \frac{L_x^2}{48} \qquad C_2 = \frac{L_y^2}{48} \qquad C_3 = \frac{L_x^2L_y^2}{2304} \qquad C_4 = \frac{L_x^4}{1280} \qquad C_5 = \frac{L_y^4}{1280}$$

With in-plane analysis, system of equation (3.30) has the following form

$$B_{11}^s(a_1 - a_2C_2) - D_{11}^s a_0 - D_{12}^s b - 2A_{66}^s C_3b_0\left(\frac{a_0b_0}{2} + a_2 + b_2\right) - M_x = 0$$
$$- D_{12}^s a_0 + B_{22}^s(b_1 + b_2C_1) - D_{22}^s b_0 - 2A_{66}^s C_3a_0\left(\frac{a_0b_0}{2} + a_2 + b_2\right) - M_y = 0$$
$$- A_{11}^s(a_1 + C_2a_2) + B_{11}^s a_0 - A_{12}^s(b_1 + C_1b_2) + N_x = 0$$
$$- A_{12}^s(a_1 + C_2a_2) + B_{22}^s b_0 - A_{22}^s(b_1 + C_1b_2) + N_y = 0$$
$$- A_{11}^s(C_5a_2 + C_2a_1) + B_{11}^s a_0C_2 - A_{12}^s(C_3b_3 + C_2b_1) +$$
$$- 2A_{66}^s C_3(2a_2 + 2b_2 + a_0b_0) + C_2N_x = 0$$
$$- A_{12}^s(C_3a_3 + C_1a_1) + B_{22}^s b_0C_1 - A_{22}^s(C_4b_3 + C_1b_1) +$$
$$- 2A_{66}^s C_3(2a_2 + 2b_2 + a_0b_0) + C_1N_y = 0$$

where

$$C_1 = \frac{L_x^2}{12} \qquad C_2 = \frac{L_y^2}{12} \qquad C_3 = \frac{L_x^2 L_y^2}{144} \qquad C_4 = \frac{L_x^4}{80} \qquad C_5 = \frac{L_y^4}{80}$$

$$(N_i, M_i) = \int_{-h/2}^{h/2} Q_{ij[eq]} v_j (1, z) dz$$

$$A_{IJ}^s, B_{ij}^s, D_{ij}^s) = \int_{-h/2}^{h/2} Q_{ij[eq]} (1, z, z^2) dz \qquad (i, j = 1,2,6)$$